8-11-2020

INTEGRATED STUDY OF LIVER FIBROSIS: MODELING AND CLINICAL DETECTION

Hao Chen

INTEGRATED STUDY OF LIVER FIBROSIS: MODELING AND CLINICAL DETECTION

by

HAO CHEN

Under the Direction of Yi Jiang, PhD.

ABSTRACT

The liver is a vital organ that carries out over 500 essential tasks, including fat metabolism, blood filtering, bile production, and some protein production. Although the structure of the liver and the role of each type of cells in the liver are well known, the biomedical and mechanical interplays within liver tissues remain unclear. Chronic liver diseases are a significant public health challenge. All chronic liver diseases lead to liver fibrosis due to excessive fiber accumulation, resulting in cirrhosis and loss of liver function. Only early stage liver fibrosis is reversible. However, early-stage liver fibrosis is difficult to diagnose. How the progression of fibrosis changes the mechanical properties of the liver tissue and altering the dynamics of blood flow is still not well understood. The objective of this dissertation is to integrate the understanding of liver diseases and mechanical modeling to develop several models relating liver fibrosis to blood flow. In

collaboration with clinicians specialized in hepatic fibrosis, we integrated computational modeling and clinicopathologic image analysis and proposed a new technology for early stage fibrosis detection. The key results of this research include: (1) A mathematical model of liver fibrosis progression connecting the cellular and molecular mechanisms of fibrosis to tissue rigidity; (2) A novel machine learning-based algorithm to automatically stage liver fibrosis based on pathology images; (3) A physics model to illustrate how the liver stiffness affects the blood flow pattern, predicting a direct relationship between fibrosis stage and ultrasound Doppler measurement of liver blood flow; (4) Statistical analysis of clinical ultrasound Doppler data from fibrosis patients confirming our model prediction. These results lead to a novel noninvasive technology for detecting early stages of liver fibrosis with high accuracy.

INDEX WORDS: Liver, Liver fibrosis, Machine learning, Blood flow, Grading

INTEGRATED STUDY OF LIVER FIBROSIS: MODELING AND CLINICAL DETECTION

by

HAO CHEN

A Dissertation Submitted in Partial Fulfillment of the Requirements for the Degree of

Doctor of Philosophy

in the College of Arts and Sciences

Georgia State University

2020

INTEGRATED STUDY OF LIVER FIBROSIS: MODELING AND CLINICAL DETECTION

by

HAO CHEN

Committee Chair: Yi Jiang

Committee: Jun Kong

Vladimir Bondarenko

Alton Farris III

Electronic Version Approved:

Office of Graduate Services

College of Arts and Sciences

Georgia State University

July 2020

DEDICATION

Thanks to my family and dear friends, without their support and encouragement, this research would not have been completed. I dedicate this dissertation to them.

ACKNOWLEDGEMENTS

I gratefully acknowledge my adviser, Professor Yi Jiang, for her superior scientific guidance and mentoring. She shows me an inspiring research picture and leads me to explore science. Thank you for supporting me kindly and patiently. I also extend my gratitude to my committee members: Professors Jun Kong, Professor Vladimir Bondarenko and Professor Alton Farris, for their insightful and valuable comments. I would like to express my appreciation to all members of the Dr. Jiang group for providing helpful discussions. Also, many thanks to my clinical cooperators from Shijiazhuang Fifth Hospital, Shanghai Zhongshan Hospital, and Guangzhou Zhongshan University Third Hospital.

TABLE OF CONTENTS

LIST OF TABLES

LIST OF FIGURES

LIST OF ABBREVIATIONS

HCV	Hepatitis C Virus
NASH	Nonalcoholic Steatohepatitis
HSCs	Hepatic Stellate Cells
ECM	Excess Extracellular Matrix
NAFLD	Nonalcoholic Fatty Liver Disease
HMGB1	High Mobility Group Box Protein 1
HAV	Hepatitis A virus
HBV	Hepatitis B Virus
ALH	Alcoholic Hepatitis
ABMs	Agent-based Models
LOX	Lysyl Oxidase
HAI	Histological Activity Index
TE	Transient Elastography
BDW	Blood Wave Ultra-Graphy
PV	Portal Vein
LHV	Left Hepatic Vein
MHV	Middle Hepatic Vein
RHV	Right Hepatic Vein
HGB	Hemoglobin
PLT	Platelet
ALT	Alanine Aminotransferase
AST	Aspartate Aminotransferase

GGT	Gamma Glutamy1 Transpeptidase
ALB	Albumin
GLB	Globulin
DBIL	Bilirubin
BUN	Blood Ureanitrogen
sCr	Serum Creatinine
PT	Prothrombin Time
INR	International Normalized Ration
ROC	Receiver Operating Characteristic

1 INTRODUCTION

Liver fibrosis arises from chronic liver damage[1]. Late-stage fibrosis, or cirrhosis, affects liver functions and is a significant public health problem[2]. The liver fibrosis is mainly induced by many reasons, including alcohol abuse, chronic hepatitis C virus (HCV) infection, toxin, and nonalcoholic steatohepatitis (NASH)[3, 4]. The fiber deposition distorts the hepatic architecture, and the subsequent development of hepatic fibrosis defines cirrhosis[5-7]. Cirrhosis is a condition in which the liver loses function due to long-term damage and causes the hepatic insufficiency and portal hypertension, respectively[8-12].

Hepatic fibrosis was historically known to be a passive and irreversible disease due to the collapse of hepatic parenchyma and the abundant fibrous tissue[13-17]. Fibrosis describes a progression in which the injured tissue was replaced or encapsulated by collagen. These responses result in the continuation of fibrogenesis. Presently there is no effective treatment for liver fibrosis[16, 18]. In the 1970s, the clinical reports first presented that the liver has the potentially reversible ability in advanced liver fibrosis[19]. With the increasing understanding of the liver structure, the function cells, including Kupffer cell and hepatic stellate cells (HSCs), were defined as the primary activity cells for producing collagen in the liver[20, 21]. Liver fibrosis is a complex process involving multiple time scales, biomechanical mechanisms, physical interaction, including cell-cell and cell-matrix, and intracellular signal transduction[22-24]. A thorough review of the process is given in Chapter II. However, how fibrosis progression affects the medical properties of the liver is not thoroughly understood and the mechanism of altering the dynamics of blood flow is still unclear. In this work, we analyze clinical data to understand the progression of liver fibrosis and develop a novel method for noninvasive diagnosis.

We simulate the fibrosis progression *in silico* and develop explanatory models at tissue and organ levels. The experimental data include biopsy and ultrasound images from our collaborators. We get the spatial information from biopsy: the fiber locations in a liver, the position of fiber relative to the vein at various fibrosis stages. The corresponding time-dependent information such as blood flow velocity and frequency in hepatic veins is extracted from the ultrasound image of the same patient. Integrating the spatial-time information improves the understanding of the dynamics of blood flow in liver and related fibrosis process.

Currently, the exact number of liver fibrosis patients worldwide is unknown but expected to be enormous. The cirrhosis patients were estimated at 400,000 in the USA[25]. This number exclude the high prevalence of undiagnosed cirrhosis in both NASH and viral hepatitis. In some Asian countries, alcohol liver fibrosis and viral hepatitis B occur at an even higher rate than in Europe. In 2015, up to 75% of cirrhosis patients had liver cancer. Due to the challenge of early-stage fibrosis detection, the actual number should be much higher than what we have [26]。

In clinical cases, liver fibrosis, especially at its early stages, is highly asymptomatic and unalarming till obvious symptoms of liver diseases develop [27]. Patients hardly pay close attention without any pathological feature. Liver fibrosis is usually detected from elastography, liver disease suggestion, and biopsy [28-30]. The accuracy of early-stage detection using elastography is at question. The diagnosis of fibrosis from suggesting liver diseases depends on the doctor's experience. About one fifth of patients with HCV take high risk to make biopsy. Thus, a liver fibrosis diagnosis method that is convenient, highly accurate, offering low cost and low risk has long been sought after.

This dissertation tries to understand the principle mechanism of liver fibrosis and build models to solve the problems in clinical liver fibrosis diagnosis. Our work develops a model to

describe the progression of liver fibrosis, including the behavior of dead cells and the distribution of fiber. The model demonstrated the details of fiber growth and produced a key to explain the blood flow in liver fibrosis stages. The blood flow model analyzes the dynamics of blood and liver fiber interaction. Using the model, we investigate the mechanisms responsible for promoting liver fibrosis. In the investigation, the liver biopsy is the standard reference. To increase the accuracy of the grading of the liver biopsy, we introduce machine learning to train the tissue slices.

The dissertation is organized by the following story. Chapter II describes a background of the biological processes and blood flow relevant to liver fibrosis topic. The chapter highlights the dead cell as a key to enable the fibroblast and hepatic stellate cell (HSC) to progress liver fibrosis. Then the structure of the fiber and hepatic vein was discussed in a different stage of liver fibrosis.

Chapter III presents an overview of mathematical modeling techniques. The models try to describe the progression of liver fibrosis within whole biological systems, and to study the dynamics of liver tissue at varying time scales. This chapter also reviews previous mathematical models of liver fibrosis and identifies their strengths and limitations. The advantage of the pixels model and the bead-spring model we used can display hepatic fiber activity more clearly. The blood flow model is based on the premise of fiber-cell interactions during liver fibrosis. These interactions are regulated at the sigla cell level.

Chapter IV presents a new machine learning method for auto-grading liver fibrosis via biopsy. The clinical and mathematical research in liver fibrosis based on biopsy introduces the need of accurate biopsy liver fibrosis grading. Currently, the classification of liver fibrosis stage was scored by the Ishak system and METAVIR system. However, the accuracy of grading depends on the experience of doctors, so the new grading method using machine learning, building on the logical reasoning of fiber growth, is designed to promote the diagnostic accuracy and reduce test

time. Our machine learning model converts the qualitative criteria into quantitative scores in the liver biopsy characterization.

Then in Chapter V, the first prospective study applies a blood flow model for staging liver fibrosis in patients. The extended model was produced and validated against diagnosis from liver biopsy. Thus, the model study how the fiber influences the dynamics of blood and thus the grading of liver fibrosis. In this chapter, the existing methods of liver fibrosis are also introduced. The newly proposed algorithms in this work analyze the ultrasound Doppler images from hepatic fibrosis patients. Liver biopsy is usually used as the gold standard reference for pathology liver fibrosis grading, as well as other references such as elastography and biomarkers, were employed to test the accuracy our diagnostic method. The results support the hypothesis of our models. We then briefly discuss the dynamics of blood flow, and propose a new noninvasive diagnostic tool for liver fibrosis.

The summary chapter VII discusses the impact and outlook of this research.

2 BIOLOGICAL BACKGROUND OF LIVER

2.1 Liver fibrosis

Liver fibrosis, the accumulation of excess extracellular matrix (ECM) in the liver, is characteristic of most chronic liver diseases, including chronic hepatitis B or C viral infection, alcoholic abuse, and nonalcoholic fatty liver disease (NAFLD), or nonalcoholic steatohepatitis[3, 31-34]. Liver fibrosis is the consequence of injury to the healthy liver. Chronic injury leads to progression of fibrosis, which eventually results in the loss of liver function. Currently, the diagnostic of liver fibrosis is based on medical imaging and liver biopsy[37]; however, there is no effective detection to quantitatively measure the stage of liver fibrosis, especially at early stage.

The gold standard for diagnosis of liver fibrosis is a liver biopsy. The Ishak scoring system and METAVIR scoring system are used to grade the stage of liver fibrosis [Table 2.1-1]. Liver fibrosis is classified into four stages by the Ishak system or METAVIR system, F1, F2, F3, and F4, respectively[4, 35, 36]. F0 is no fibrosis. The early stage of liver fibrosis is F1-F2. The advanced liver fibrosis is F3-F4. When fibrosis progresses to architecture with the formation of fiber, it is considered cirrhosis (F4).

Table 2.1-1 ISHANK and METAVIR scoring system for liver fibrosis[38].

Ishak stage: Categorical description	ISHAK	METAVIR
No fibrosis (normal)	0	F0
Fibrous expansion of some portal areas ±short fibrous septa	1	F1
Fibrous expansion of most portal areas ±short fibrosis septa	2	F2
Fibrous expansion of most portal areas with occasional portal to portal (P-P) bridging	3	
Fibrous expansion of portal areas with marked bridging (portal to portal (P-P) as well as portal to central (P-C)	4	F3
Marked bridging (P-P and/or P-C), with occasional nodules (incomplete cirrhosis)	5	
Cirrhosis, probable of definite	6	F4

2.1.1 Liver biopsy

The biopsy is treated with the gold standard of liver fibrosis reference and assessed the grading of inflammation and staging of fibrosis. However, the biopsy is limited to diagnosis sampling variability in all liver diseases [4, 39-41]. Thus, the accuracy of biopsy diagnosis only achieved 65% and 75% when the sampling size is 15mm and 25mm in length, respectively[4].

Despite this shortcoming, the biopsy is still required to grade liver fibrosis and to provide its cause. Only the clear signs of cirrhosis do not need the biopsy confirmation of fibrosis, such as ascites and coagulopathy[42].

A liver biopsy is obtained by the larger-diameter needle under the ultrasound guidance[43, 44]. Each patient usually is cut at least two times, to get more sampling variability. The suction needle is used to prevent tissue fragmentation[45].

2.2 The mechanism of Liver Fibrosis

The formation mechanism of cirrhosis is progressive fibrosis. The collagen of healthy hepatic tissue mainly distributes around the portal area and central vein[46, 47]. During the fibrosis, collagen observably increases and deposit in the lobules. At cirrhosis, the liver loses function due to the forbidden of exchange between vessel and liver cells[28].

2.2.1 Hepatic tissue

At the hepatic fibrosis condition, although the fibrosis tissue forms many little bands, they still aren't fully connected. When fibrosis continues to progress, the fiber bands will bridge to each other to rebuild the lobule of structure.

At the healthy condition, the liver is divided at the histological scale as lobule by vein, and the pattern of the lobule is hexagon in two-dimensional (Figure 2-1). In the lobule, there are vessels, hepatocyte, Kupffer cell, fibroblast, hepatic stellate cell, and collagen. The function of the vessel is transporting nutriment and cells[48]. Typically, Kupffer cells transport in liver tissue through the vessel. Kupffer cells are characteristic macrophages located in the wall of the sinusoid, which is a small blood vessel in the liver, and the activation is responsible for the liver injury[49-51]. Fibroblast is a type of cell which synthesizes ECM and collagen[52]. Hepatic stellate cells are found in a small area between the sinusoids and hepatocytes and also is activated by cytokines

(Figure 2-2). Collagen is the main structural protein in ECM and displays a triple helix chain[53]. In the liver, myofibroblasts are function cell which produces excessive amounts of collagen in wound tissue[54], and then the wound concomitant alignment of the collagen fibers by integrin-mediated pulling on the collagen bundles[55].

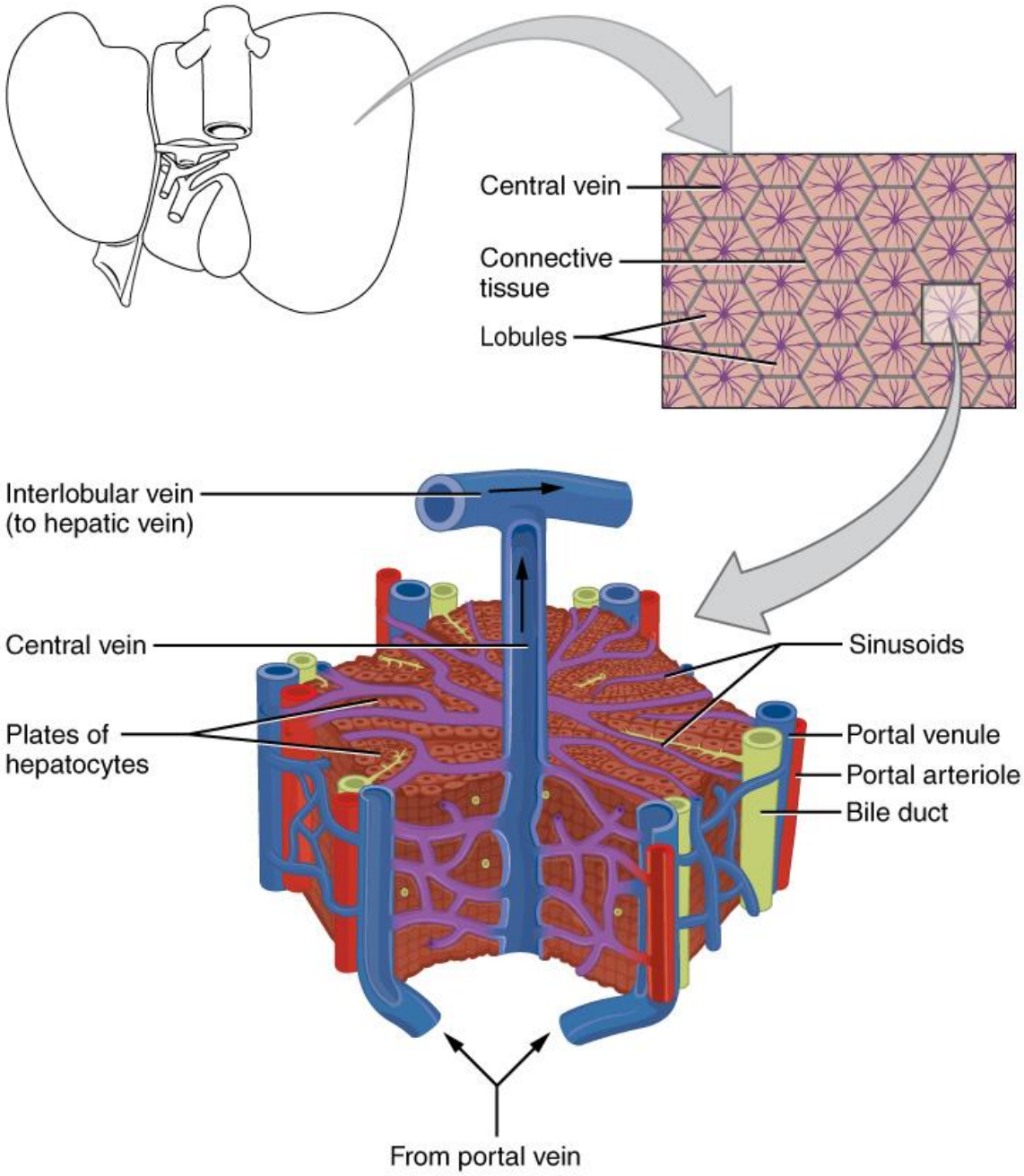

Figure 2-1 Microscopic anatomy of the liver. The hepatic lobule is building the liver tissue, consisting of central vein, sinusoids, portal field and plates of hepatocytes[56]. This image are licensed under a Creative Commons Attribution 4.0 International License.

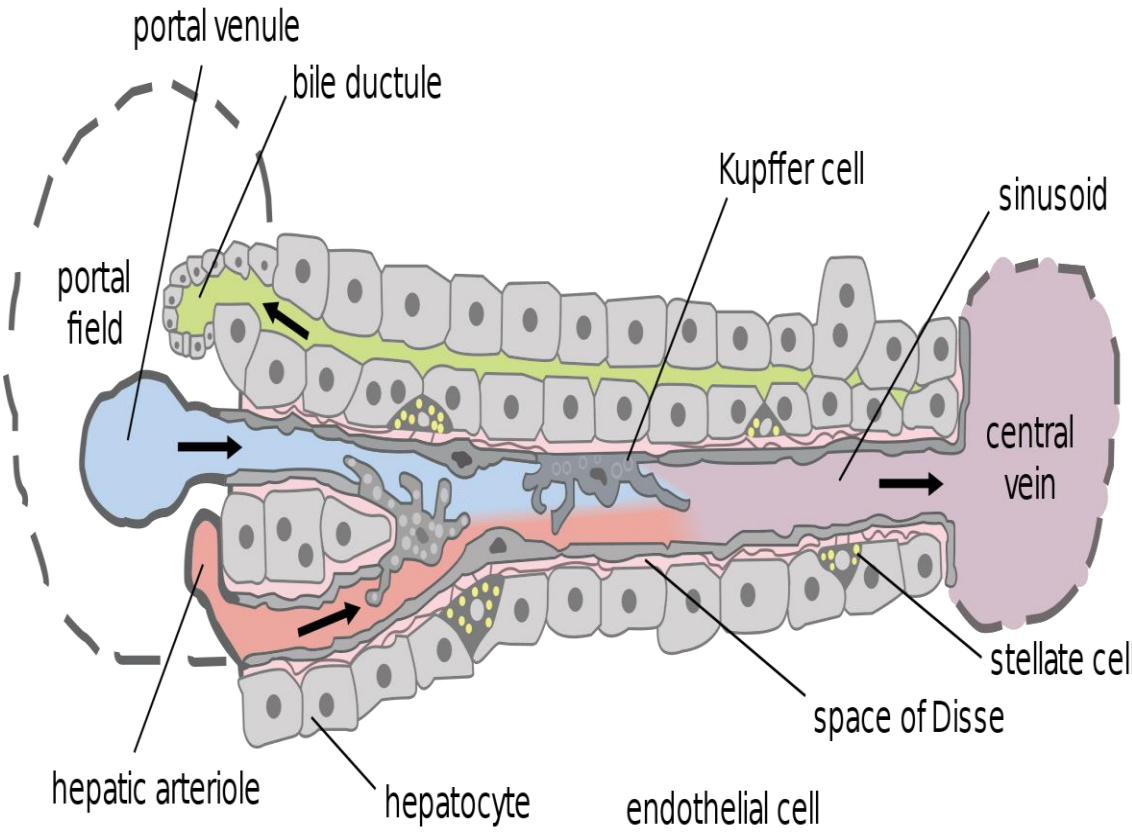

Figure 2-2 The mammalian liver. Portal field includes portal venule, hepatic arteriole and bile ductule. The Kupffer cell is lining in the sinusoid and release cytokines. The disse is a space between the sinusoid and the hepatocytes. [57].

2.2.2 Kupffer cell

In the liver, injury and toxicity transforms hepatic cells to the dead agent. The function of Kupffer cell is surveying the area and phagocytizing dead cells and producing the cytokines in the process[49, 58]. The cytokines are TNF-α and TGF-β1[59]. Biologically, inadequate clearance of dead cells can lead to liberating some damage-associated molecular pattern molecules such as high mobility group box protein 1 (HMGB1)[60].

In the liver, the cellular damage due to liver injured leads to the upregulation and release of damage-associated molecules such as HMGB1[61]. HMGB1 attracts the Kupffer cells to phagocytose dead cells and produce cytokines, including TNF-α and TGF-β1 in the process[62].

HMGB1 and TNF-α can effectively activate fibroblast and HSC to induce their transformation to myofibroblast. TGF-β1 makes myofibroblast proliferation and deposition of ECM. Figure 2-3 summarizes the cellular mechanisms of the fibrosis process[63].

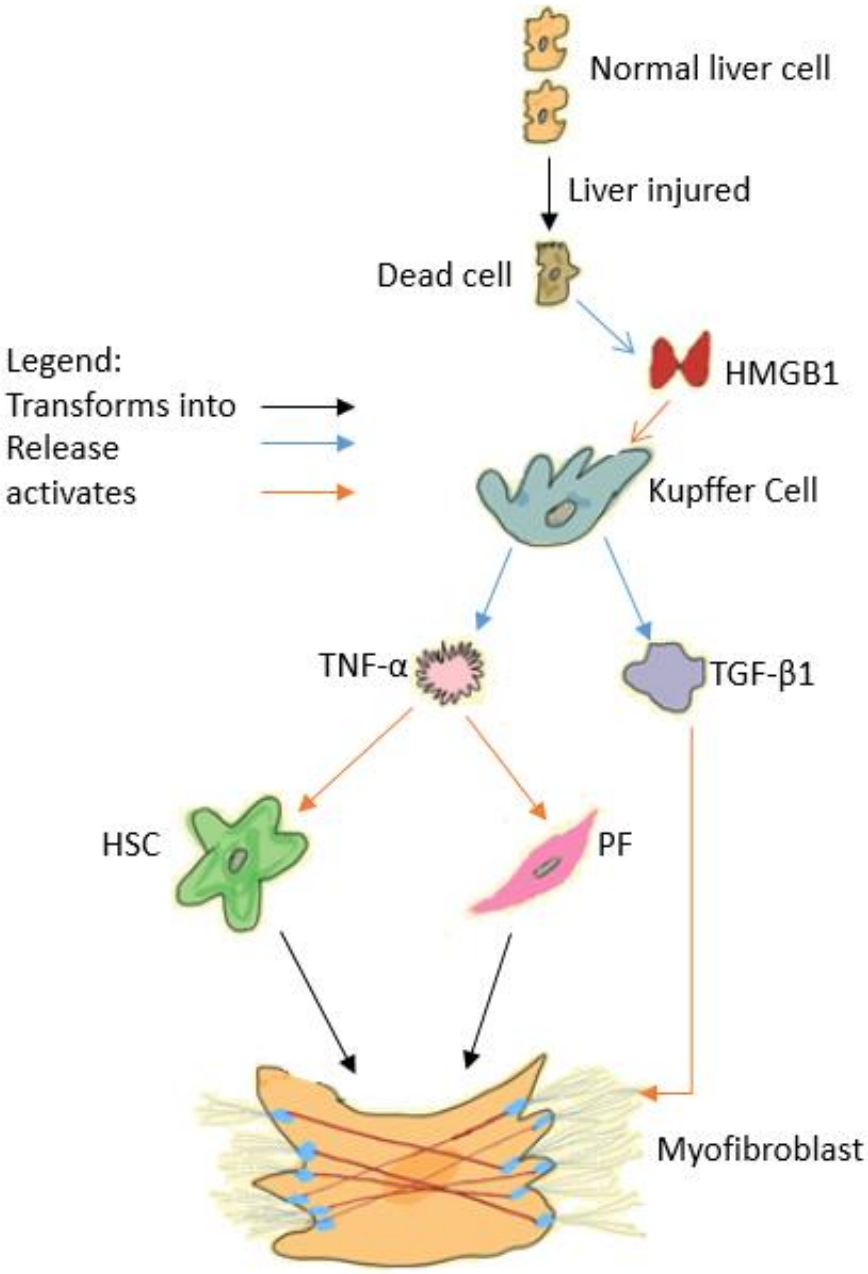

Figure 2-3 An overview of cellular and molecular mechanisms of myofibroblast activation and fibrosis.

2.2.3 Collagen

Collagen is the main structural protein in ECM and displays a triple helix chain. Most of the collagen molecules are assembled in the form of long thin fibrils of similar structure. In contrast, collagen type-IV forms a two-dimensional reticulum. The basic structural unit of collagen is a triple helix, which is a long (300nm), thin (1.5 nm diameter) protein[64]. All collagen is due mainly to segments to connect each other by chemical activity and then fold into different kinds of three-dimensional structures[65].

2.2.4 Collagen interactions and fibrils

Many three-stranded collagen molecules bundle together to form fibrils side by side with 50-200 nm[66]. In fibrils, about one-quarter of the length of collagen molecules is connected. So the characteristic pattern of the collagen bundle is repeated such staggering array.

Short segments on the collagen chains play a critical role in the formation of collagen fiber. These short segments are just short chains and contain special amino acid hydroxylysine. Covalent aldol cross-links are formed by lysyl oxidase and oxygen[67] (Figure 2-4). And these covalent cross-links keep this side-by-side collagen chain stability and generate a strong fibril (Figure 2-5).

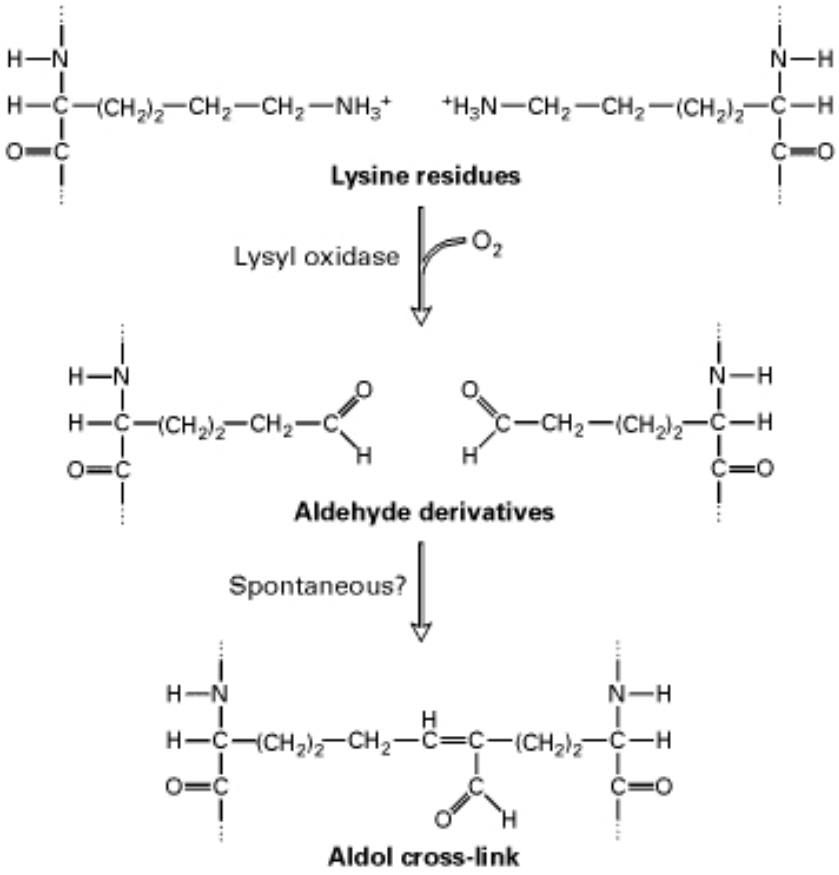

Figure 2-4 The generation of aldol cross-link[67]. Used with permission.

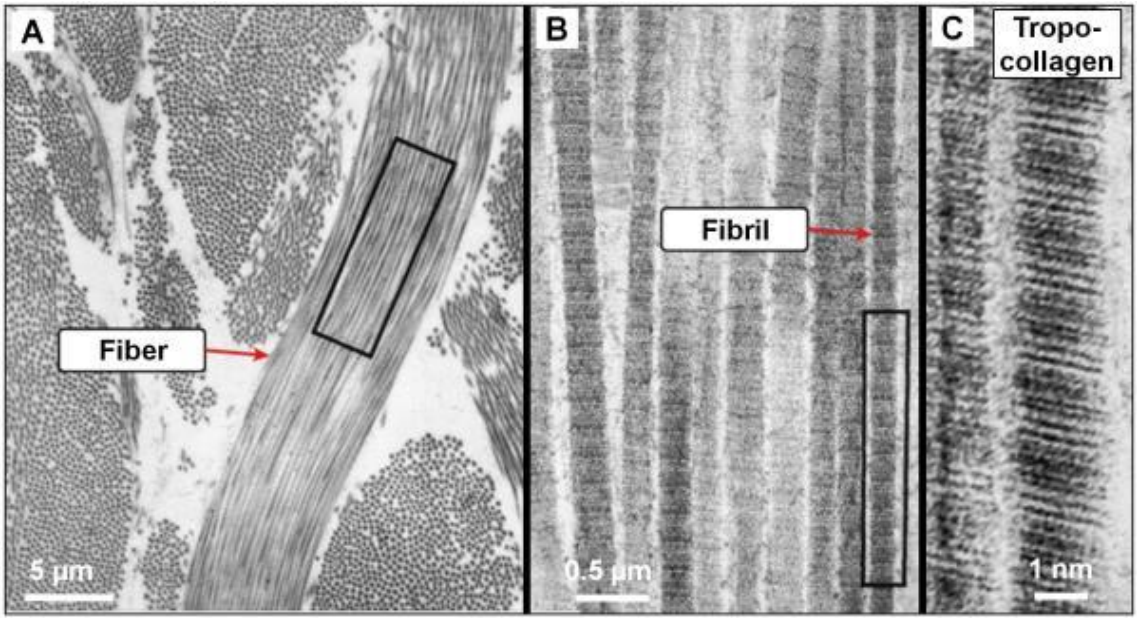

Figure 2-5 Collagen chains. A. collagen fibers, B. Collagen fibril, C. the tropocollagen molecule[68]. Histology @Yale

Collagen fibrils which have tremendous tensile strength are packed side by side in parallel bundles to form collagen fibers. So, in collagen structure, there is no crosslinker, all collagen fibrils are connected by covalent cross-links.

2.2.5 The macro-pattern of collagen

The pattern of the lobule is the hexagon, which is divided by veins in the liver[69]. In cirrhosis, lots of collagen fibrils segments replace the dead cells, which are around the vein to form collagen bundles by covalent cross-links. The distribution of collagen fiber follows the vessel structure. In two dimensional, the pattern of collagen bundle is hexagonal. In three-dimensional, the structure of the collagen bundle looks disordered. However, all the collagen bundles spread from the boundary of the lobule to the central vein.

3 MODELING LIVER FIBROSIS

Liver fibrosis has been a significant challenge in public health. However, the change of mechanical properties of liver tissue is still a myth. Integrating the understanding of liver fibrosis, we built a mechanical model for the liver. The model simulates the toxin diffusion in the liver that leads to hepatic tissue damage and collagen deposition. Also, we used the bead-spring model to test the mechanical properties of the liver during fibrosis. The mathematical models and simulation results can be used as a research tool to synthesize in-depth research for the liver.

Liver fibrosis is a wound healing response in which damaged liver regions are encapsulated by an extracellular matrix or scar. Chronic liver injuries can be caused by a viral infection, toxin exposure, NASH, an autoimmune disorder, and metabolic disorders[70] and physical injury.

Viral hepatitis commonly refers to the hepatitis A virus (HAV), hepatitis B virus (HBV) and hepatitis C virus (HCV)[71-73]. HAV is caused by contaminated food or water. HBV and HCV are infected by body fluids. HAV and HCV are RNA viruses. HBV is a DNA virus. They activate CD4+T cells to transfer to serval kinds of subtype T cells, which have a different function[74]. The activated T cell can produce inflammatory cytokines[75]. The inflammatory cytokines such as IL-17 and IL-22 promote liver fibrosis by activating hepatic stem cells (HSCs), which regulate chemokines and fibrogenic genes or result in hepatocellular damage[76-79]. Hepatitis virus enters the liver through blood, then influence the liver health[80]. The earliest infected cell was discovered around the portal area (Figure 3-1)

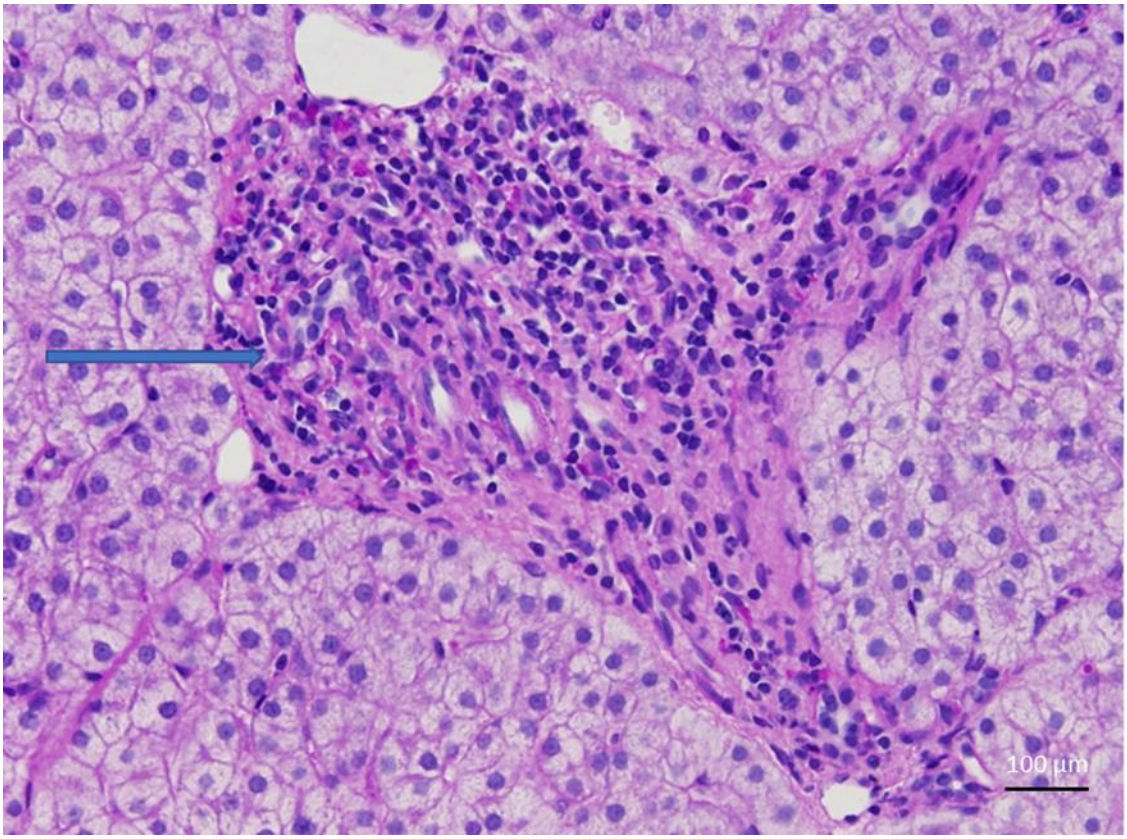

Figure 3-1 Liver biopsy shows inflammation and interface hepatitis. The arrow points to eosinophil clusters. Image courtesy of Dr. Ye Lihong from Shijiazhuang fifth hospital.

In the United States and Japan, alcohol is the primary cause of liver fibrosis. Almost 10% - 35% of heavy drinkers have alcoholic hepatitis (ALH)[28]. While an alcoholic cannot directly relate to the development of hepatic fibrosis, this action seems more popular than others in liver disease. With chronic ethanol intake, gut-derived endotoxin was absorbed into the portal circulation. In the early stage of ALH, the activated Kupffer cells produce pro-inflammatory cytokines and chemokines, which result in liver injury. Then macrophage and neutrophils are increased by those chemokines and cytokines in fatty liver and steatosis (figure3-2). The amplified systemic inflammation and immunodeficiency from alcoholic hepatitis patients were observed.

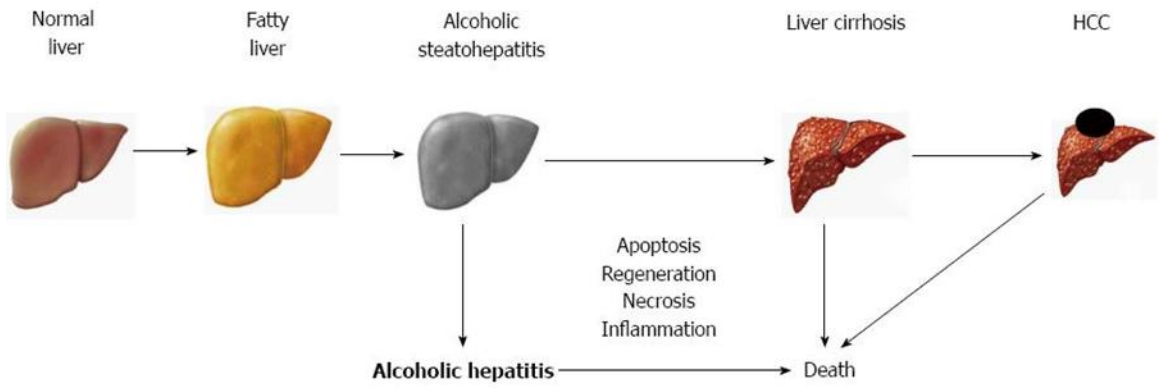

Figure 3-2 Illustration of alcoholic liver disease progression [81].

Endotoxin was produced because of impaired cytotoxic function [82]. The endotoxin leads to a high injection rate in alcoholic hepatitis patients. It enters the liver through bile. Based on the direction of bile flow, the concentration of endotoxin in bile is highest in the central of the lobule.

Nonalcoholic steatohepatitis (NASH) is another reason to result in liver cirrhosis. It leads to a fatty liver that is not caused by alcohol. It is caused by a metabolic disorder, malnutrition, and industrial poisoning [83].

In summary, the deposition of collagen fibers starts from the portal area in most hepatitis diseases. In this project, we model the progression of liver fibrosis as a result of toxic substance.

3.1 Existing models

Currently, there is no comprehensive mathematical model for liver fibrosis. One model by Ying et al [84] only focus on one stage of cirrhosis by the simple structure. They developed a model and predict the elastic behavior and its modulus evolution of cirrhotic human liver comparing with experiment data. They derived modulus evolution for the strain energy function through mathematics by using cubic structure[84] (Figure 3-3).

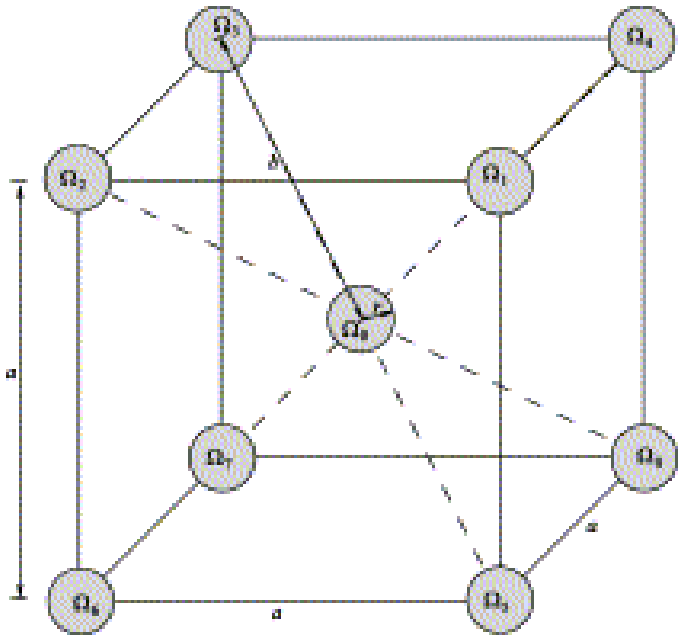

Figure 3-3 Eight-particle interaction model of composites for deformation. They assume the matrix and particle have the isotropic elasticity tensors.[84].

Another published model also describes the liver fibrosis process. Vodovotz's research use to translational systems biology to generate and simulate the liver fibrosis processes[85]. Park et al. tried to study the changes in drug disposition properties due to liver disease using a normal and diseased version of abstract, agent-oriented In Silico Livers (ISL), and validated the models' mechanisms against disposition data from rat livers, normal and diseased. They dynamically traced the disposition differences for diltiazem and sucrose across five levels, mapping to measure of histopathology, and thus measured disease-causing differences in local ISL effects. The model can explore how hepatic drug disposition differs in less or more advanced stages of liver diseases, contributing to unraveling the complex correlation between liver disease and drug disposition.[89]. Bhattacharya et al. studied chemical- and drug-induced toxicity via "toxicity pathways" using computational systems biology approaches. They described three case studies in computational modeling approaches to understand perturbation of intracellular toxicity pathways on toxicity of

the liver (hepatotoxicity), including Computational systems biology pathway (CSBP) models, ordinary differential equations (ODEs), and Agent-based modeling (ABM). These computational models can determine toxicity pathways and improve dose-response estimation.[90]. Wambaugh and Shah proposed a graphical model of the sinusoidal network to simulate a spatially extended hepatic lobule, integrating in vitro liver experiments with agent-based cellular models. They aim to develop a framework to quantitatively and efficiently simulate the microanatomic distribution of various chemicals in a canonical lobule for time period ranging from hours up to months. They assumed a discrete topological architecture of the hepatic via a graphical model, to explicitly explore the concentration distribution of environmental chemicals. Then materials flow one-dimensionally through sinusoidal elements of transformed network. Thus the relationship between individual exposure and microdosimetry is estimated by connecting the virtual lobule to a physiologically-based pharmacokinetic (PBPK) model. The method provides a possibility to cheaply access variable inter- and intracellular chemical dynamics with potential to alter lobule geometry. The limitations are biologically additional data such as information on the statistical distribution of lobule morphology and the cell response to local chemical levels is needed. Besides, whether three-dimensional lobule paradigm in simulation is needed remains unknown.[91]. Friedman et al. focused on the biochemical regulations of fibrosis[92], using a system of partial differential equations to explore the efficacy of potential drugs in the progression of liver fibrosis.

To simulate the progression of fibrosis, one would need to describe the details at the sub-lobular scale. The agent-based models (ABMs) is a very popular model aiming to test the hypotheses regarding dynamic changes in several arears of clinical interests[86-88]. Joyeeta et al. built a multiscale agent-based model to compute liver inflammation on a structural skeleton of

physical forces[93]. The model used agents representing hepatocytes and collagen to test any changes in size or elasticity in liver fibrosis.

The previous models mainly focus on elastic behavior and the concentration of drug in liver fibrosis. Our model is built for viral inflammation leading to liver fibrosis, which starts to affect how the inflammatory substance diffuse in the liver and how the fiber grows following the distribution of dead hepatic cells. The model will perform the whole progression of fiber growth which is from inflammatory substance diffusion. The simulation images will be used to compare the real liver tissue and join the training group for machine learning.

3.2 Pixel – diffusion model

Our biophysical model of liver tissue is approximated to cell death because of toxin diffusion. The simulation of liver fibrosis has two models using pixel-diffusion model and bead-spring model. Pixel-diffusion model is used to describe the dynamics of toxin spreading from a hepatic vein using biological rules that dictate their behaviors. Toxin diffusion evolves at a constant rate and responds to the distance to the hepatic vein. The concentration of the toxin changing environment leads to the death of hepatic cells. From a simple set of rules, Pixel-diffusion model can exhibit highly complex phenomena. With the increasing understanding of the biological system, the realistic and relevant model becomes more command to increase the level of description. In supporting the computational ability of computers, Pixel-diffusion model preforms the whole process of toxin spread with solving Pixel-diffusion models. Bead-spring model describes the physical properties of liver tissue with the finite element method (FEM). FEM is the most comprehensive method for solving the traditional fields of structural analysis. Bead-spring model simulates the deformation of liver structure in a different stage of liver fibrosis.

3.2.1 Toxin diffusion

Our simplified biophysical model of liver tissue is approximated as a hexagonal lattice of lobules, the vertices of the hexagons correspond to portal veins, and the centroid of the hexagons are the locations of the central veins (Figure 3-4). The various research shows toxin results in hepatocyte damage and fibrosis[94-96]. In the pixel-diffusion model, the toxin as the pixel agent enters the lobule from the portal vein and flows out through the central vein. In the simulation, assuming toxic substances are small molecules that diffuse freely in the tissue, with the sources at the vertices and sinks at the centroids,

$$\frac{\partial C}{\partial t} = D\left(\frac{\partial^2 C}{\partial x^2} + \frac{\partial^2 C}{\partial y^2}\right) - \gamma C \,, \qquad (1)$$

where C is the toxin concentration, D is the diffusion coefficient, γ is the decay rate. We used MATLAB to solve this PDE, After running 1000 simulation steps, the result which approach the steady state, shows that the concentration of the substance which moving in and out of capillary walls as the blood exchanges materials with hepatic cells depends on the distance to the portal vein (Figure 3-5). In the simulation, we varied the initial concentration of toxin at portal vein, also set D and γ in the model. The initial concentration of toxin relate to how much toxin in the portal vein. The diffusion coefficient D is a constant which doesn't depend on the density and describe the diffusion rate of toxin in a given region over time.

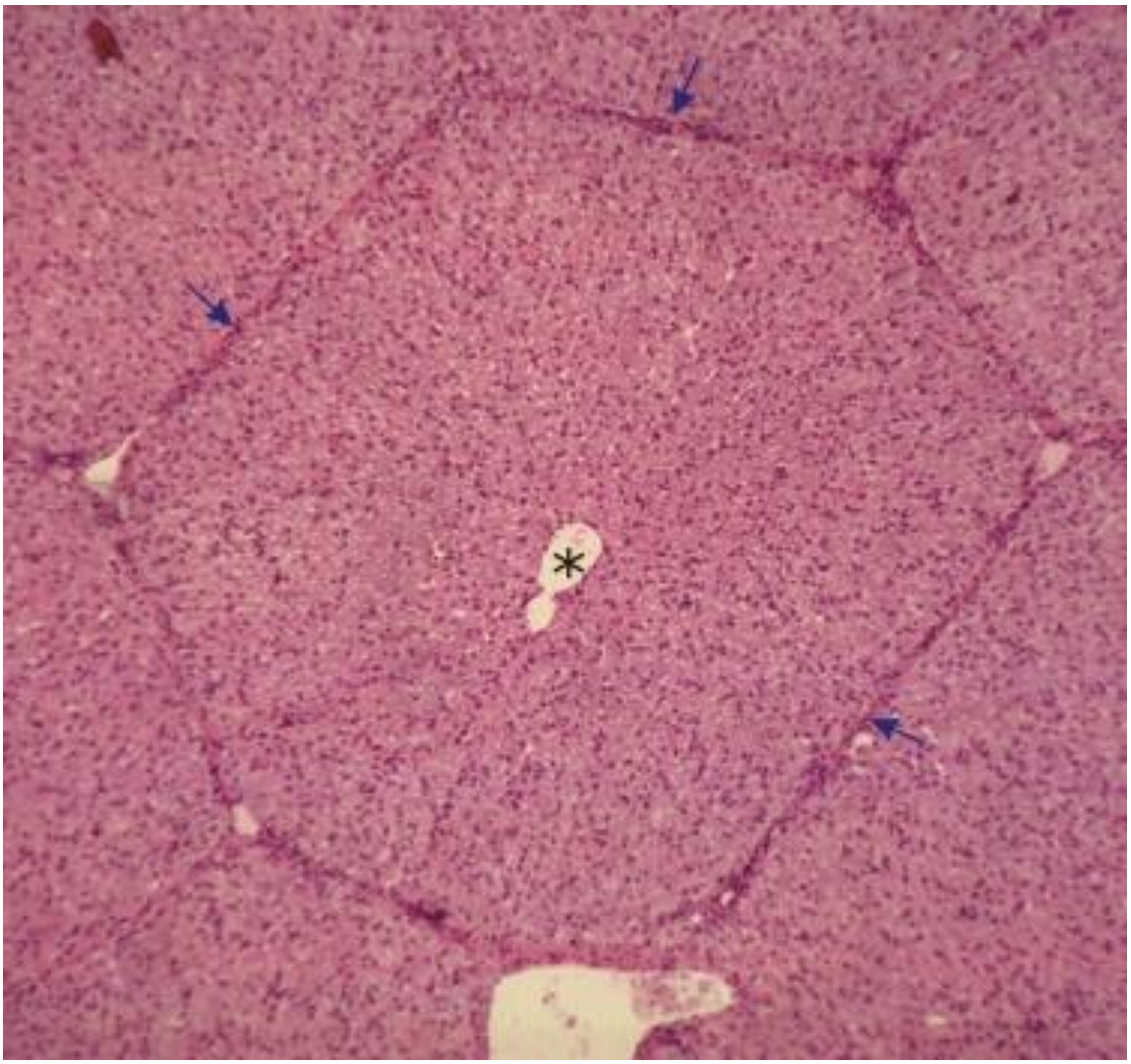

Figure 3-4 The hexagon of liver lobules. The central vein (*) is in the center of the hexagonal lobule. The arrow refers to the boundary of the lobule. The vertices of the hexagon are vessels (i.e., portal veins, hepatic arteries, and ducts). The tissue was stained with H-E.[97].

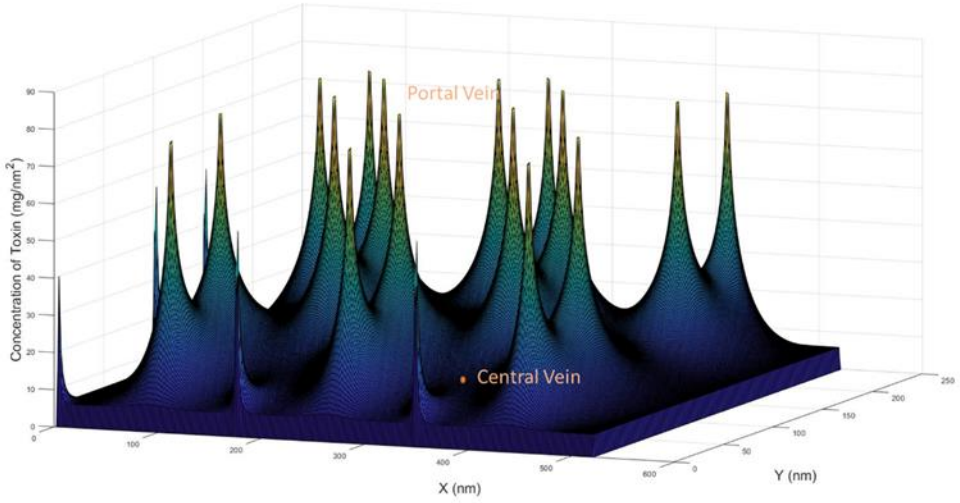

Figure 3-5 The concentration of toxin as thesolution of Equation with 1000 simulation steps(1). Concentration of toxin is c in equation (1). The concentration of toxins represented in height.

We further assume that cell damage is linearly proportional to the concentration. The pattern of activation of myofibroblasts is the same as the concentration field. Hence the production and deposition of the collagen also follow this concentration pattern. The collagen forms fiber by fiber, stochastically.

3.2.2 The death of the hepatic cell

The process of hepatic fibrosis evolves at the interaction of toxin and the death of the liver cell. Cell death results in fiber deposited by myofibroblast; meanwhile, it also describes why the fibers encapsulate the lobule at first. In our model, the hepatic cell was introduced to the regeneration function, and the dead cell has a high probability to appear in portal area. The model assumes that some hepatic cells die due to the toxin damage at each unit time. The nearest dead cell from the vein is kept, and the others are regenerated to be hepatic health cells. In the code of simulation, we assume that hepatic cells die when the concentration of toxin exceeds a threshold

value. The threshold value depends on the toxin type and affects the elastic of liver tissue. Previous experimental studies used a toxin to induced liver injured and indicated the progression of liver fibrosis in response to hepatic injury[92] (Figure 3-6). In the figure, the infected cells were distributed around portal vein and form a connect channel between two portal veins, which like our simulation result.

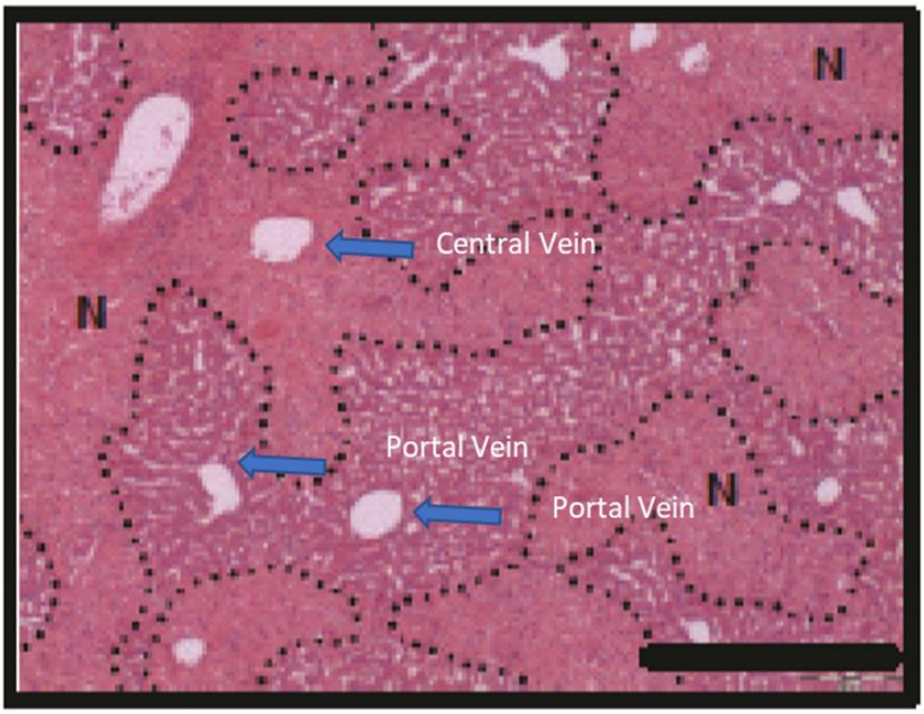

Figure 3-6 H&E staining of liver tissue. Necrotic areas are marked by dotted lines. Black bars represent 0.5 mm[92].

3.3 Bead–spring model

The structure of bead-spring model was derived from pixel-diffusion model results. After each simulation step, the pixel of the dead cell will transfer to fiber pixel because of the interaction of myofibroblast. The number of fiber pixels that were calculated in the small area defines the stiffness of unit length. The calculating area was defined by the threshold of concentration of toxin in pixel-diffusion model. The area was divided into segments by the portal vein. In bead-spring

model, a complex spring was used to simulate the stiffness of liver tissue. We assume the number of total pixels in a limit area is np, the number of fiber pixels is nf, the original stiffness coefficient of spring is f, the stiffness coefficient of fiber spring is f_{fiber}, so the stiffness coefficient of complex spring is

$$f_c = \frac{n_p - n_f}{n_p} f + \frac{n_f}{n_p} f_{fiber}$$

The crosslinker proteins, e. g. lysyl oxidase (LOX) is assumed to be uniformly distributed, which forms covalent bonds between fibers. In the mechanical model, we assume each joint between fibers/springs is cross-linked.

We use complex spring to represent the mechanical of the fiber bundle network as fibrosis progresses. (Figure 3-7) In the liver fibrosis, the black spring was combined with tissue spring and fiber spring. The elastic of coefficient for the black spring is

$$k_{spring} = \frac{k_{fiber} + k_{tissue}}{k_{fiber} k_{tissue}} \quad ,$$

where k_{spring} is the elastic coefficient for spring, k_{tissue} is the elastic coefficient for tissue and k_{fiber} *is the elastic coefficient for fiber*.

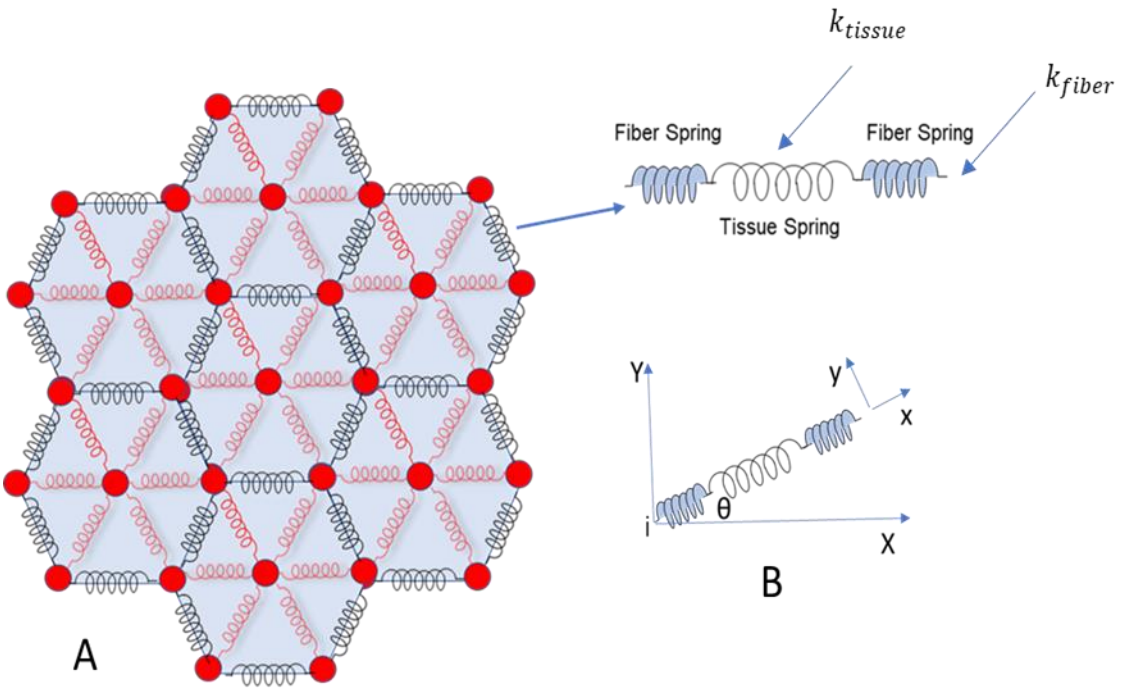

Figure 3-7 A: An illustration of a 2D mechanical pattern described as a bead-spring model. The red beads are each joint to show typical chain behavior. Black springs correspond to collagen fibers distributed around the boundary of the lobules. Red springs present elastic tissue property.B: The dimensional of the spring.

To simulate mechanical property change in the liver tissue during the progression of liver fibrosis, we build a bead-and-spring model. Each spring has a Young's modulus E, area of cross-section of spring A and length L between two nodes (l, j). θ is the intersection angle between the vector $\vec{\iota j}$, and vector $\overrightarrow{X_\iota}$. (Figure 3-11) Assuming $C = cos\theta$ and $S = sin\theta$, so the element stiffness matrix is [98]:

$$k = \frac{EA}{L}\begin{bmatrix} C^2 & CS & -C^2 & -CS \\ CS & S^2 & -CS & -S^2 \\ -C^2 & -CS & C^2 & CS \\ -CS & -S^2 & CS & S^2 \end{bmatrix}$$

Since each element has 4 degrees of freedoms (each node has two degrees freedoms: x and y), the whole stiffness matrix K should be 2n×2n, following

$$\{K\}\{U\} = \{F\}$$

U is the displacement vector of the node; F is the load vector of the node.

The force of each element can be got from

$$f = \frac{EA}{L}[-C \quad -S \quad C \quad S]\{u\}$$

Where f is the force of the element node. Then the displacement of each node is

$$u = \frac{k}{f}$$

Through bead-spring model, the elastic stiffness of liver tissue was measured by calculating Young's modulus in the model. An external force was applied to the top and bottom boundaries of a tissue (Figure 3-8). Based on our calculation algorithm, each node has a displacement at each time step. A higher Young's modulus value would show a more flexible condition of the tissue. Since the deformation of tissue requires the external physical force that could affect the following structure of simulation, the force value as a parameter in the model was changed to measure the elasticity of tissue.

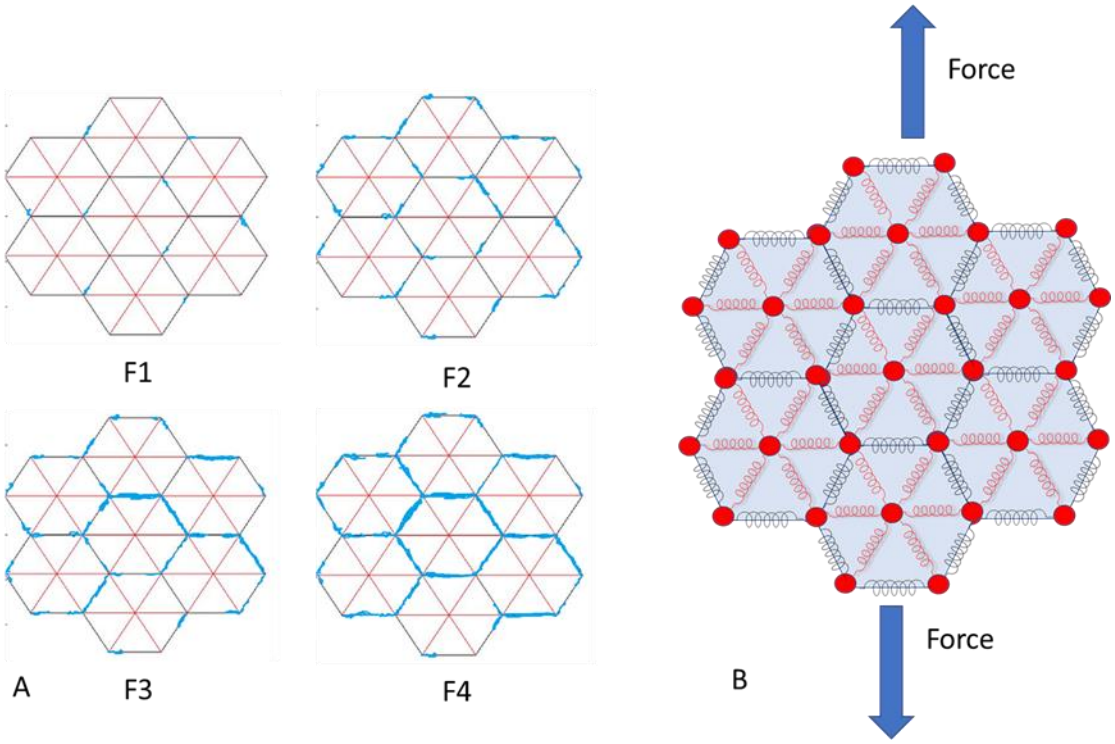

Figure 3-8 A. The fiber randomly growth in the tissue. Red line is tissue structure. Blue region is fiber. B. Applied forces stress the liver tissue.

3.4 Results

In pixel-diffusion model, we calculate the concentration of toxin at each point. The higher concentration of toxins has a higher potential of leading to a dead cell. Dead cells leads to fiber deposition, which eventually form the pattern of the fiber bundle.

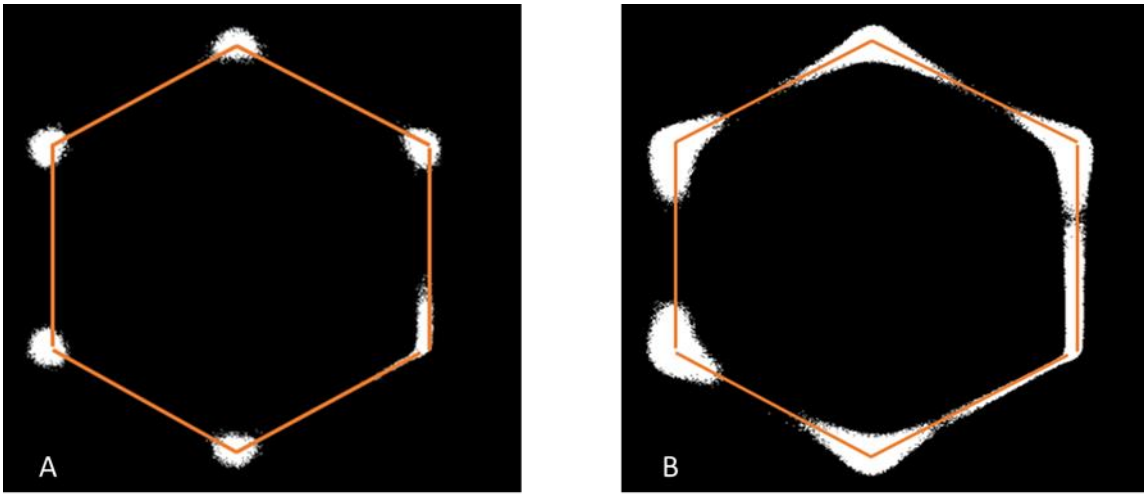

Figure 3-9 Dead cell mapping in the progress of toxin diffusion at one simulation step. The white points correspond to fiber pixels. means dead cells. orange lines outline the lobule (Hexagon). A is early stage of liver fibrosis. B is heavy stage of liver fibrosis.

In Figure 3-9, the concentration of dead cells around portal trails is higher than in other areas, and the concentration at the boundary of the lobule is also higher than the central vein. That means the fiber begins to be released around portal trails, and then collagen deposited to construct the fiber bundle to separate the single lobule. Based on the understanding of the process of fiber filed, the simulation shows the gradual development of the fiber patterns, which in time enclose the lobule. As hepatocytes died in response to high level toxin, persistent damage the fiber deposition in the dead cell region.

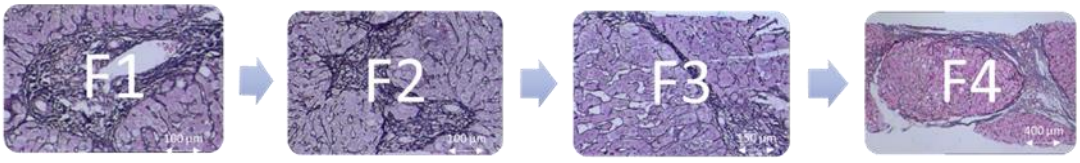

Figure 3-10: Representative histology images from the liver biopsy with Masson stain, show each stage of hepatic fibrosis. Collagen and elastin fibers were stained blue. The hepatic cell was stained red. Courtesy of Dr. Wang Zhengyan of Shijiazhuang 5Th Hospital, China.

In figure 3-10, the definition of grading for liver fibrosis in the simulated fiber images still follows the METRIA system. At the F1 stage, the fibers were deposited around the portal vein. Then, fiber bundles were found in stage 2. After fiber bundles bridging two portal veins, the simulation enters the 3rd stage of liver fibrosis. In stage 4, fiber bundles closed the whole lobule.

After converting the fiber pixel map to the bead-spring model, the liver tissue was strained by force in different stages of hepatic fibrosis, the young's modulus of liver tissue is shown in Figure 3-11. The stiffness of the liver enhances with the fiber increase in the tissue, and the results indicate that hepatic fibrosis progression increases liver stiffness.

After converting the fiber pixel map to the bead-spring model, the liver tissue was strained by force in different stages of hepatic fibrosis. The young's modulus was used to represents the elastic of liver tissue. In the model, we vary the concentration threshold to modify the width of fiber. The width of the fiber is proportional to the stiffness of fiber. Ten stiffness levels were set into the model, and each level has the same difference with the neighbor. The liver tissue was strained by extra force under the ten levels. Each line shows Young's modulus changes with fiber growth. In figure 3-13, Young's modulus increases with time as fibrosis progression in simulation. At the same simulation time step, Young's modulus is proportional to the concentration threshold.

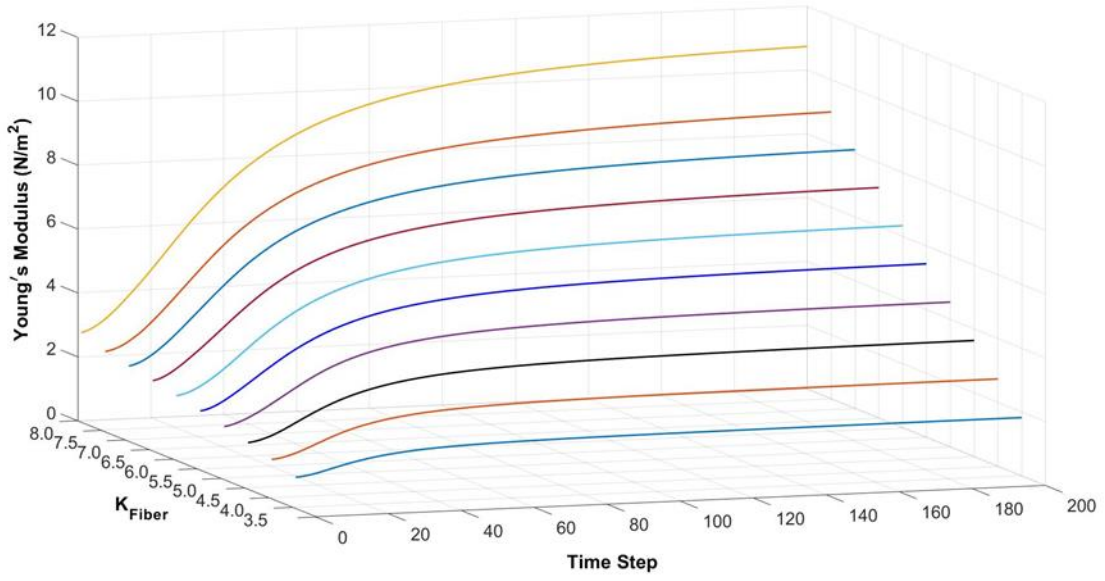

Figure 3-11 Young's modulus is varying in the fiber growth process. K_{fiber} *is the elastic coefficient of unit fiber.* $k_{tissue} = 3$

The model simulates the fiber growth in 30, 60, 300, and 1000 simulation time steps. We summarize the mean Young's modulus in each stage of liver fibrosis at each time step and make an box plot (Figure 3-12). The definition of each stage of liver fibrosis in the model follow the description of the METAVIR system. In the first stage of liver fibrosis, the fiber appears at the portal area, and the length of each fiber is less than 15% of the length of the boundary of the lobule (LBL). If the length of fiber is between 15% and 99% LBL, the liver fibrosis is in the second stage. In the third stage, the fiber bridge is formed, and the number of fiber bridge is less than 6. After the amount of fiber bridge is greater than 6, the liver is cirrhosis.

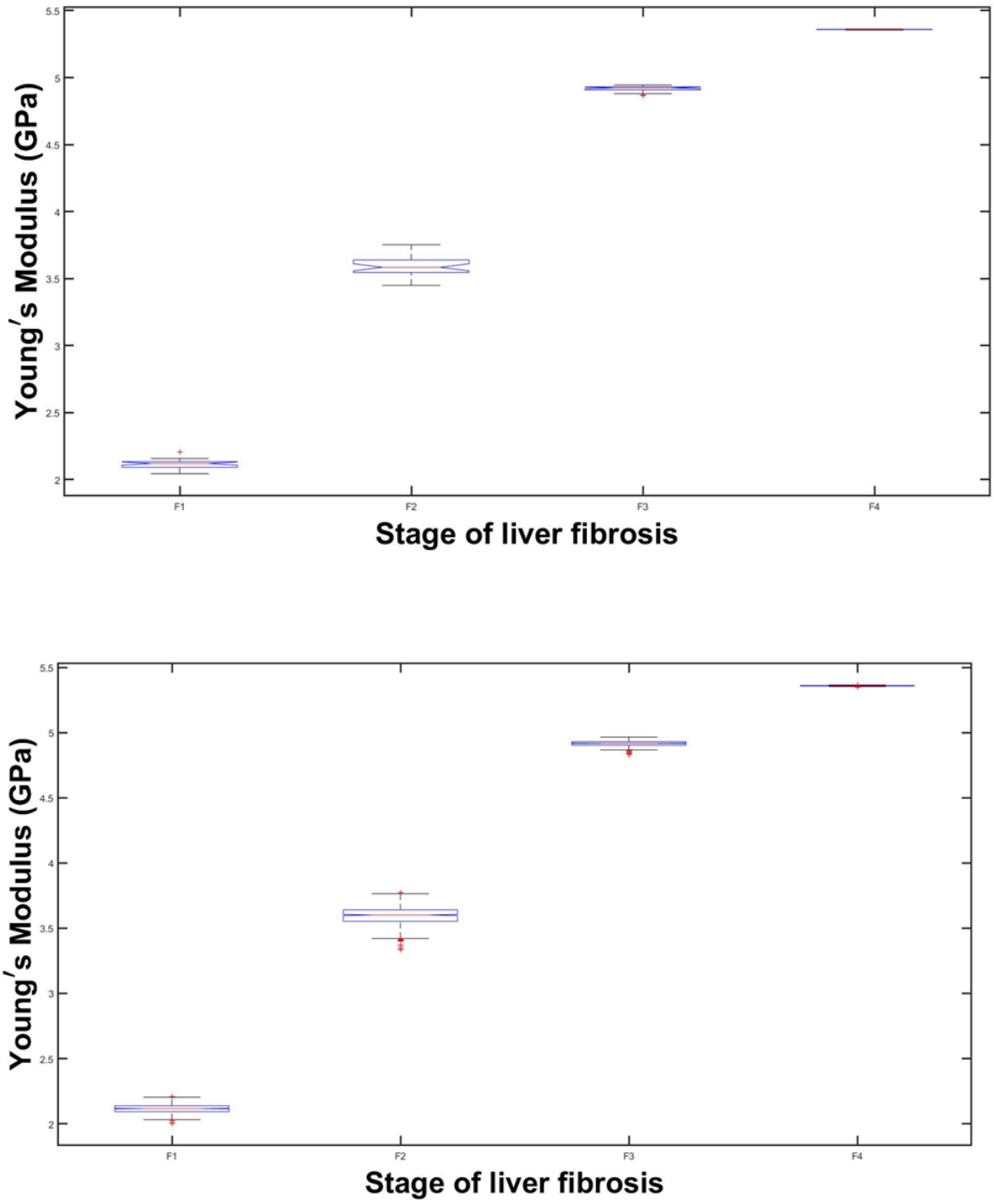

Figure 3-12 Young's modulus vs. stage of liver fibrosis. The simulation runs fiber growth in 30 times and 1000 times. Upper is 30 times and lower is 1000 times.

The fibers grow in the liver tissue randomly in 30 to 1000 times. The range of Young's modulus of liver tissue at each stage was stable after running 30 times. The stiffness of the liver enhances with the fiber increase in the tissue, and the results indicate that later stages of hepatic fibrosis correspond to increase liver stiffness. In the figure 3-15, there is not much difference between 30 times and 1000 times. The Young's modulus is stable at F4 stage, which means that the most stiffness of liver has less variability in cirrhosis and easily be measured. On the contrary, the box plots in early stage (F1 and F2) has variability and are presented with whiskers. So, the accuracy of measurement of liver fibrosis has lower accuracy in early stage.

3.5 Discussions

To determine the mechanical property change during the progression of liver fibrosis, we start from the molecular and cellular mechanisms to model toxin induced liver fibrosis. We first use a diffusion equation to describe the concentration of toxin at each point in the liver tissue. The toxin diffusion developed a model of fibrosis growth that can simulate the fibrosis progression fiber by fiber based on the underlying molecular and cellular mechanisms. The fibrosis growth model was verified through the real liver biopsy images, wherein emergent patterns are seen as defining the characteristics of liver fibrosis. The ability of a model can recreate these patterns to indicate the stage of liver fibrosis in generating. It explains the hepatic fibrosis progression and the pattern of the fiber bundle in a different stage of liver fibrosis. Then we developed a mechanical model (bead-spring model) of the liver tissue based on the fibrosis growth model that shows mechanical results consistent with our understanding of fibrotic liver.

The goal of the mechanical model was to examine the stiffness of liver tissue in fibrosis. The results reveal that the effective Young's modulus of the tissue increases as increasing amount of fiber deposited in the liver. Thus, the model was used to test hypotheses on fiber patterns and

the mechanical properties in the liver. The model described the qualitative feature of hepatic fibrosis through different fiber patterns in the biological liver tissue. Finally, from the past studies in liver tissue biomechanics, many living tissues are inhomogeneous and more complex structures{references}. Hence, our future work will focus on developing an inhomogeneous model, which can reproduce the process of liver fibrosis in three dimensional and observe the inner situation changed, such as blood flow. The work, in this chapter, represents the first step in series research to develop a toxin-based interaction for modeling the process of liver fibrosis and the mechanisms of tissue changing.

Interestingly, the low variability the Young's modulus at F4 suggests that it would be easy to detect F4 stage of liver fibrosis though the stiffness value. However, the larger variabilities in the Young's moduli at early stages of liver fibrosis means the staging based on tissue stiffness, e.g., using transit elastography, will result in higher variability and lower accuracy.

4 AUTO-GRADING OF LIVER FIBROSIS IN LIVER TISSUE SLIDES

Liver biopsy has been the gold standard evaluation for liver disease diagnoses in terms of grading or stages. Assessment of histopathological features for disease staging uses semi-qualitative scoring systems, including Metavir, Ishak, Ishak-modified system, and Histological activity index (HAI) [100],[101]. However, the scoring systems are description and subject to observing variability. [40] The accuracy of grading liver biopsy depends on the experience of the interpreter. [102] Because of these limitations, we aim to build machine learning-based algorithms for improved liver fibrosis quantification and grading using histological slides, in order to complement the pathologists.

Feature representations play an essential role in analyzing medical imaging. Based on the previous understanding of the architectural and structural feature of liver tissue in liver inflammation, it was assumed that fibers are generated around the portal area, bridging each portal vein to neighbors. [103] In grading stages of liver fibrosis, Ishak and Metavir are the two most popular grading systems and provide the estimation of liver fibrosis in liver biopsy. According to the description of the grading systems, several types of regions are observed from liver tissue, including blood vessels, capsule, structural collagen and hepatic cells. The study of all the mentioned components in an image builds the foundation of liver fibrosis analysis techniques.

Although the some papers for auto-grading liver tissue slides have been published, they mainly use observed features from images as training data in deep learning directly. [104] The observed features include fiber morphology and gray-level matrix for each pixel. These methods in deep learning demand considerable computational power and a large number of data samples. To improve the analysis efficiency of imaging and reduce the number of needed training samples, we build a new logical rule-based algorithm to provide a robust framework for liver slides

classification via machine learning. The traditional algorithms estimate grading using the manual segmentation and feature extraction from the images. Since the lack of a standardized and robust method for making slides, the small sizes of stained area, including dopant and original fiber, inferior the assessment of liver fibrosis. The new algorithm converts slide images to the array of objects. The limitations of traditional algorithms are responded by the last numbers in the range of objects, which will be reduced influence for training. Here, we evaluate our new algorithm of auto-grading liver biopsy with machine learning techniques including random forest, support vector machine, and artificial neural networks. At last, we summarize the algorithm into a web platform to support auto-grading liver tissue slide service.

4.1 Materials and Methods

Human liver tissues were scanned in Wuhan Tongji Hospital through our collaboration with Dr. Chen Yaobing A total of 492 human liver tissue slides were randomly separated into the training group and the validation group. The 393 tissue slides in the treatment group were assigned at the corresponding grading levels of F0, F1, F2, F3, and F4. The other 101 tissue slides in the control group were predicted after completing the training process.

All the liver tissues were cut into 0.5 cm sections, embedded into paraffin blocks, and made Masson trichrome staining, which is used in the histological assessment. The blocks were sectioned into slides at 4μm thickness. The tissue was mordanted in Bouin's solution for 15 minutes, and then slides were washed in running tap water to remove all the picric acid (yellow color) from sections. The sections were stained in Weigert's working hematoxylin for 10 minutes. This working solution is suitable for approximately 10 days. After rewashing the sections, the tissue was stained in Bievrich scarlet acid fuchsin. The Bievrich scarlet acid fuchsin can stain cytoplasm and muscle red. The slides were stained in Phosphotungstic/Phosphotungstic acid

solution, then rinsed in distilled water three times before placed in 1% acetic acid solution for 1 minute.

The slides images were taken with a scanner (NanoZoomer S360) using a 40X objective lens. Each image was acquired from full-size liver tissue in the slide (Figure 4-1), where pink color stains normal hepatic cell, blue color stains collagen fiber, and the white space in tissue is blood vessel.

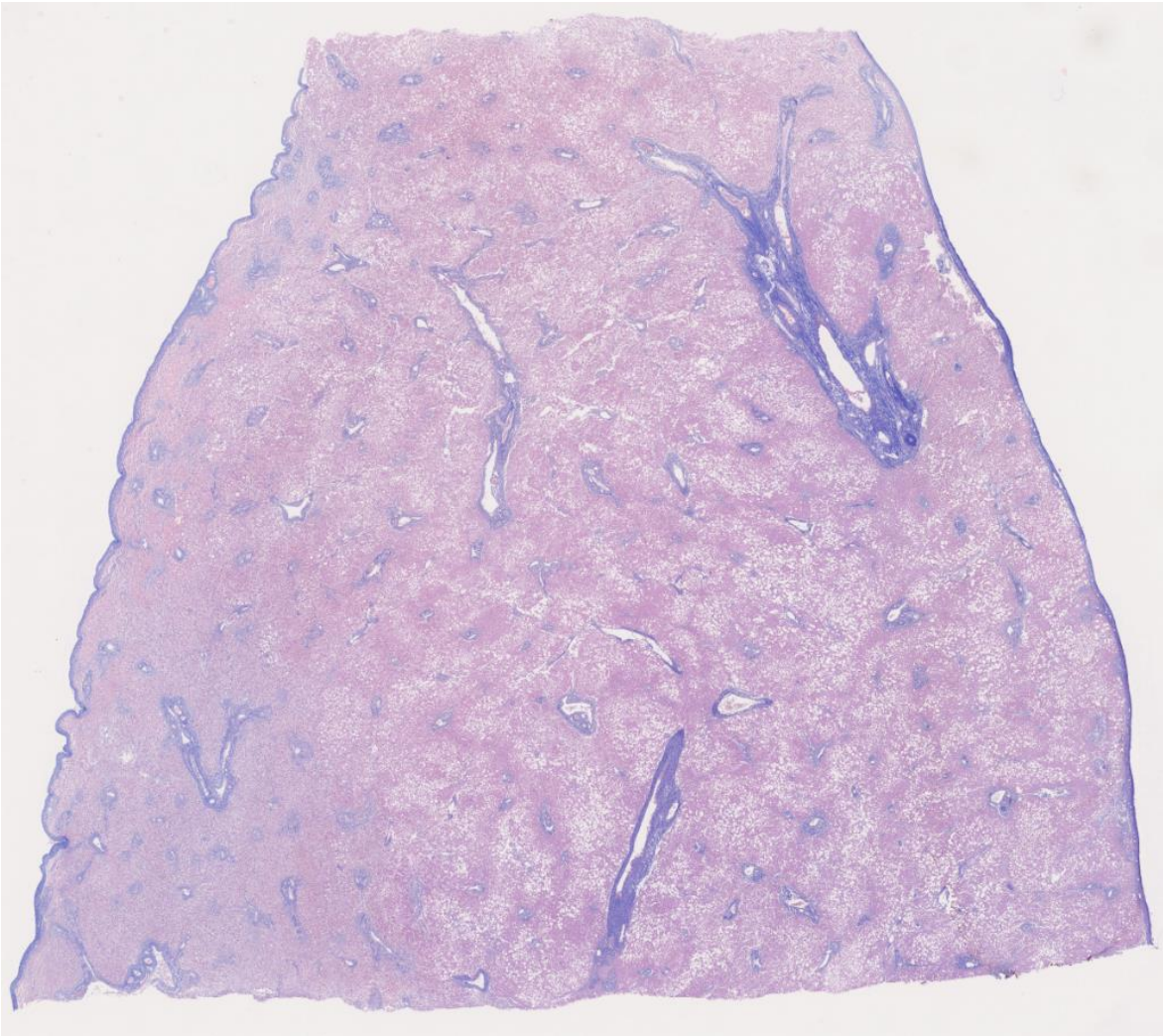

Figure 4-1 The liver tissue in slide with Masson stain. Red corresponds to the liver cell. Blue corresponds to fiber. White corresponds to the vessel. Size: 16.2mm × 12mm, 36480 pixels × 28160 pixels. Resolution: 444 nm/pixel. Courtesy of Dr. Chen Yaobing from Wuhan Tongji Hospital.

To reduce potential bias, only one pathologist graded all slides, using the Metavir scoring system. After training the samples, the accuracy is not high enough. The ineffective solution maybe caused by the less data for machine learning. Because the size of images is large, we can cut images to increase the number of training data. In order to keep accurate staging for fibrosis in each image, we only split each of the 123 liver slides equally into 4, resulting in 492 images as training samples. 4 should be the optimal number of cuts that maximize the number without sacrificing staging need. Fewer cuts could not match the model requirement. Each image was cut vertically and horizontally (figure 4-2). The samples staging distribute from F0 to F4 (Table 4.1-2). Within these samples, 9.7% of all images are F0-1. Most of patients with early stage of liver fibrosis did not have any symptoms. 47% of all images are F2, because the diagnostic for F2 stage patients mainly depends on observing their liver tissue, other non-invasive methods could not give high accuracy detection. So patients with F2 have to be sliced liver tissue for pathology. For the cirrhosis patients, the doctor can diagnose pathology through touching the liver area on the body. This is the reason why our cirrhosis images is only 17%.

Table 4.1-1 Biopsy samples distribute across fibrosis stages.

Liver Fibrosis Stage	Count	Prob
0	28	0.05691
1	20	0.04065
2	232	0.47154
3	128	0.26016
4	84	0.17073
Total	492	1.00000

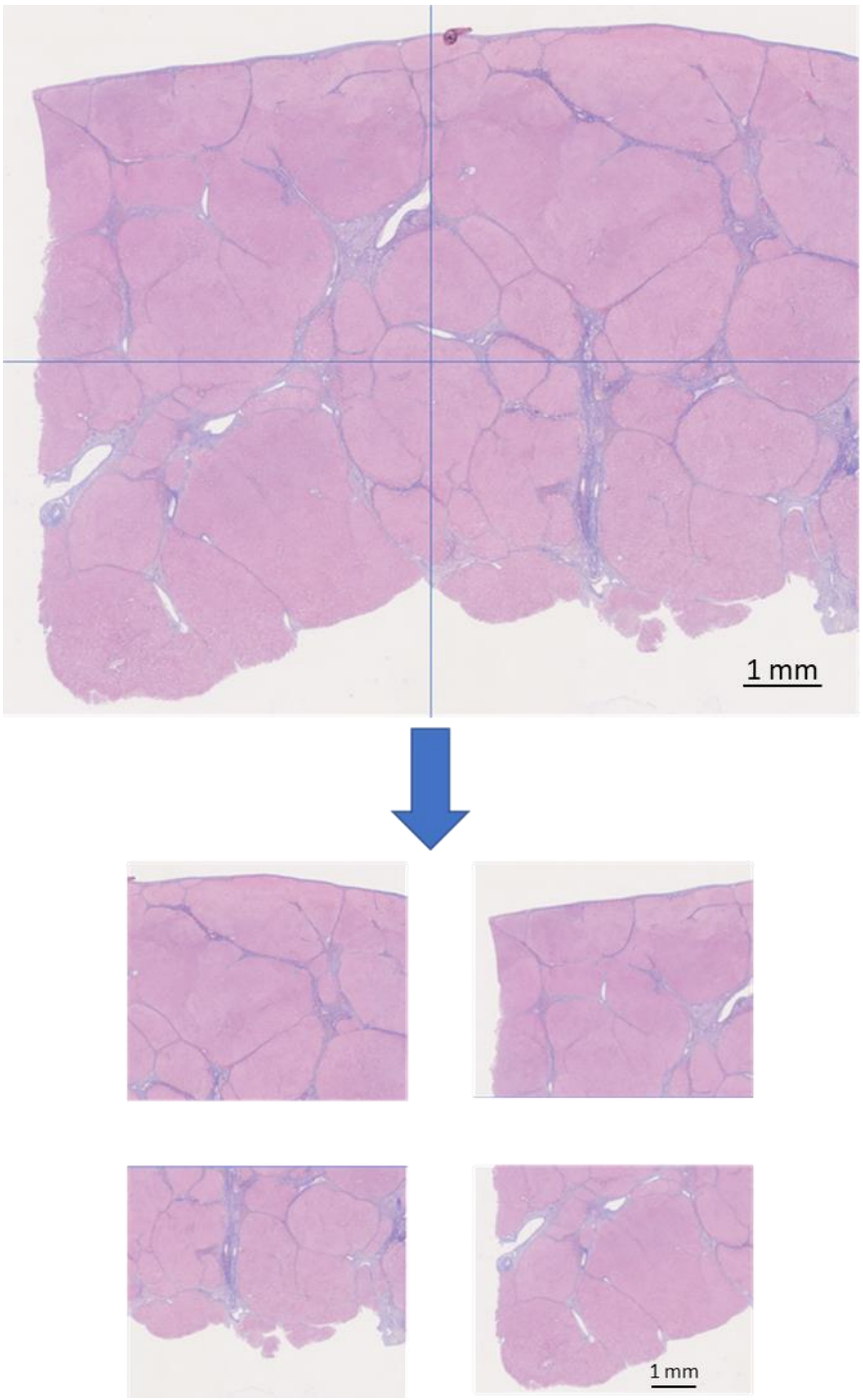

Figure 4-2 The whole image was cut into four pieces; each piece has the same stage of liver fibrosis. Resolution: 444 nm/pixel.

4.2 Features extraction

We first converted the images from NDPI to TIFF using Python, then analyzed them using MATLAB (version 2019a). We first adjusted the binary models to label the boundary of each section, and then used color deconvolution to transform color images into digital images representing the stain concentrations. The tissue/background separation is implemented using the boundary of each section. Three component types, including fiber, vessel, and fibrous, are extracted from tissue images, based on color scale grading (Figure 4-3). Due to the existence of tissue regions such as blood clots and muscle tissue, the segments of less than 220 pixels were removed to eliminate any background and steatorrhea in the cell. Also, only the largest liver tissue in the image was retained before analyzing, because the largest tissue usually have most complete information. Each tissue was classified by the boundary. The largest liver tissue has the highest number of pixels in the boundary.

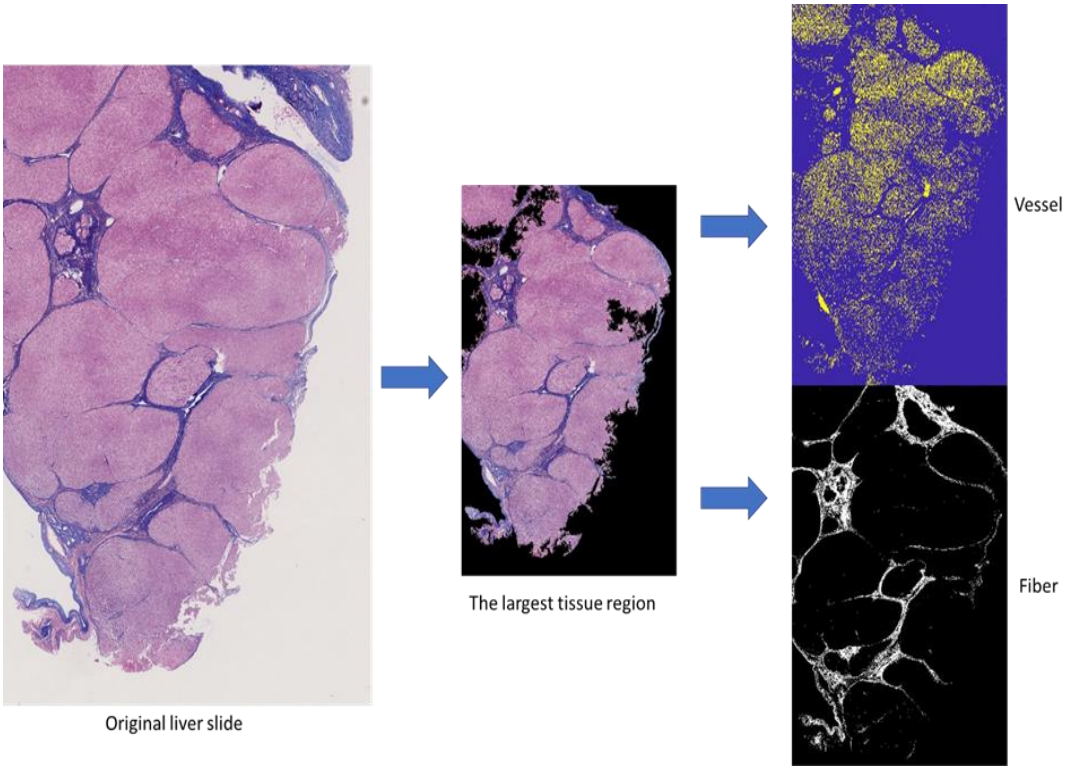

Figure 4-3. Image preprocessing. Left: Representative liver slide image with Masson stain: pink corresponds to healthy hepatic cells; white corresponds to the veins, blue corresponds to collagen fibers. Middle: background removal and noise extraction from the original liver slides. Right: (Top) Segmented image with only vessels (yellow) includes portal vein, central vein, and other small vessels, and (Bottom) Segmented collagen fiber (white).

4.3 Machine learning-based algorithm for automated fibrosis staging

The full model was derived in two steps. In the first step, the fibers and vessels were detected from each image, as input training data for machine learning algorithms. The logistical rule was summarized from the description of the Metavir scoring system. The explanation for each stage of liver fibrosis mainly discusses the spatial relationship between fiber and vessel, and the spatial distribution of the fibers. In the early stage, the fibers accumulate near the portal veins and the amount decreases with increasing distance to the portal vein. As liver fibrosis progresses, fibers form dense bundles bridging the adjacent portal veins.

Analysis treating the single vein is the original point of the new reference frame, where the fiber first appears nearest to the vein and then diffuse to occupy all around the vein. In other words, the fiber circle was built. The fiber bundles form a long rectangle, starting from the boundary of the fiber circle, centering around the vessel (Figure 4-4). So, we design a model to compare the position of fiber relative to the vein in the slides. For each slide, we calculate the distance from each fiber pixel to the center of its nearest vein and plot the distance to the vein vs. the number of fiber pixels (Figure 4-5). We assume that the stage features of liver fibrosis will manifest on the histogram of the distances. The histogram shows two steps (Figure 4-5). The first step represents the fibers near the vessel. The area under curve of the step corresponds to the number of fibers around the portal vein and thus reflects the liver fibrosis level at the early stage. The appearance of the second step is a sign that the liver begins to form fiber bundle and fibrosis develops to more severe stages. The width of the second step is the average length of fiber bundles. According to the Metavir scoring system, the conspicuous fiber bundles mean the stage enters the F2 or higher stage. We tested this algorithm using simulated image from our fibrosis model (chapter III) and produced the standard reference curves for various stages in liver fibrosis progression (Figure 4-6).

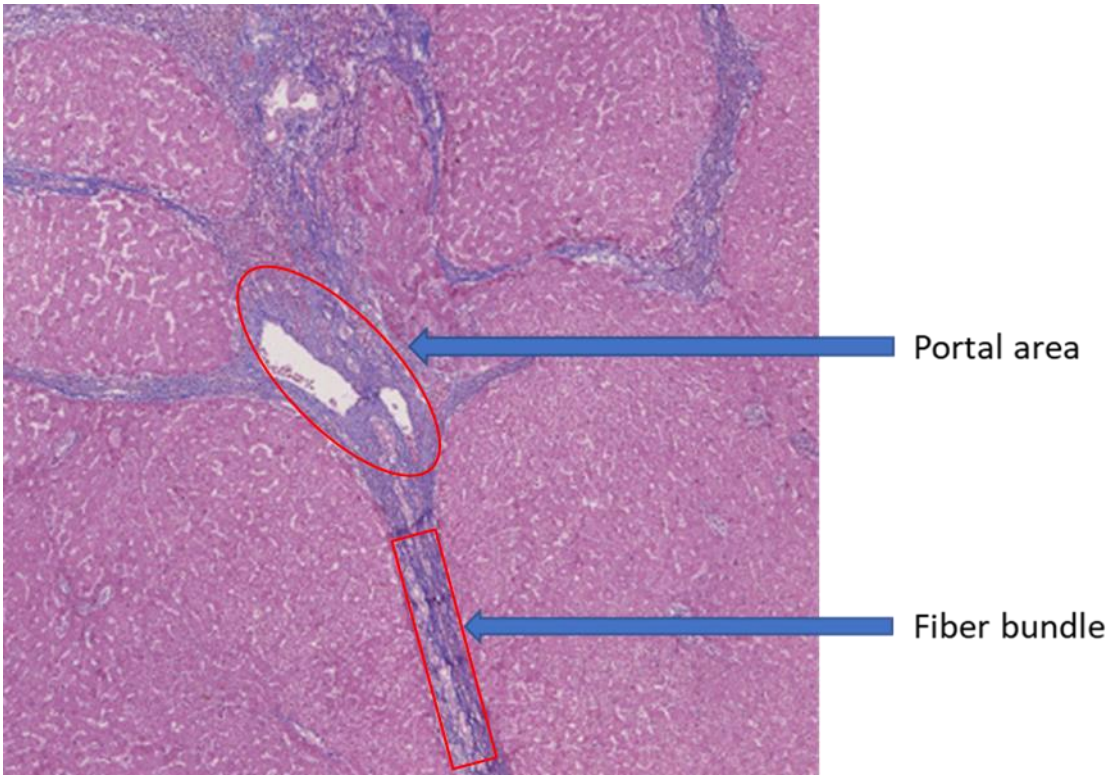

Figure 4-4 The fiber bundle forming a long rectangle starts from the portal area. The liver tissue was colored with Masson stained. Red corresponds to the liver cell. Blue corresponds to fiber. White corresponds to the vessel. The two arrows point to the portal area and fiber bundle. The red circle marks the fiber around portal area. The fiber bundle forms a rectangle. Resolution: 444 nm/pixel.

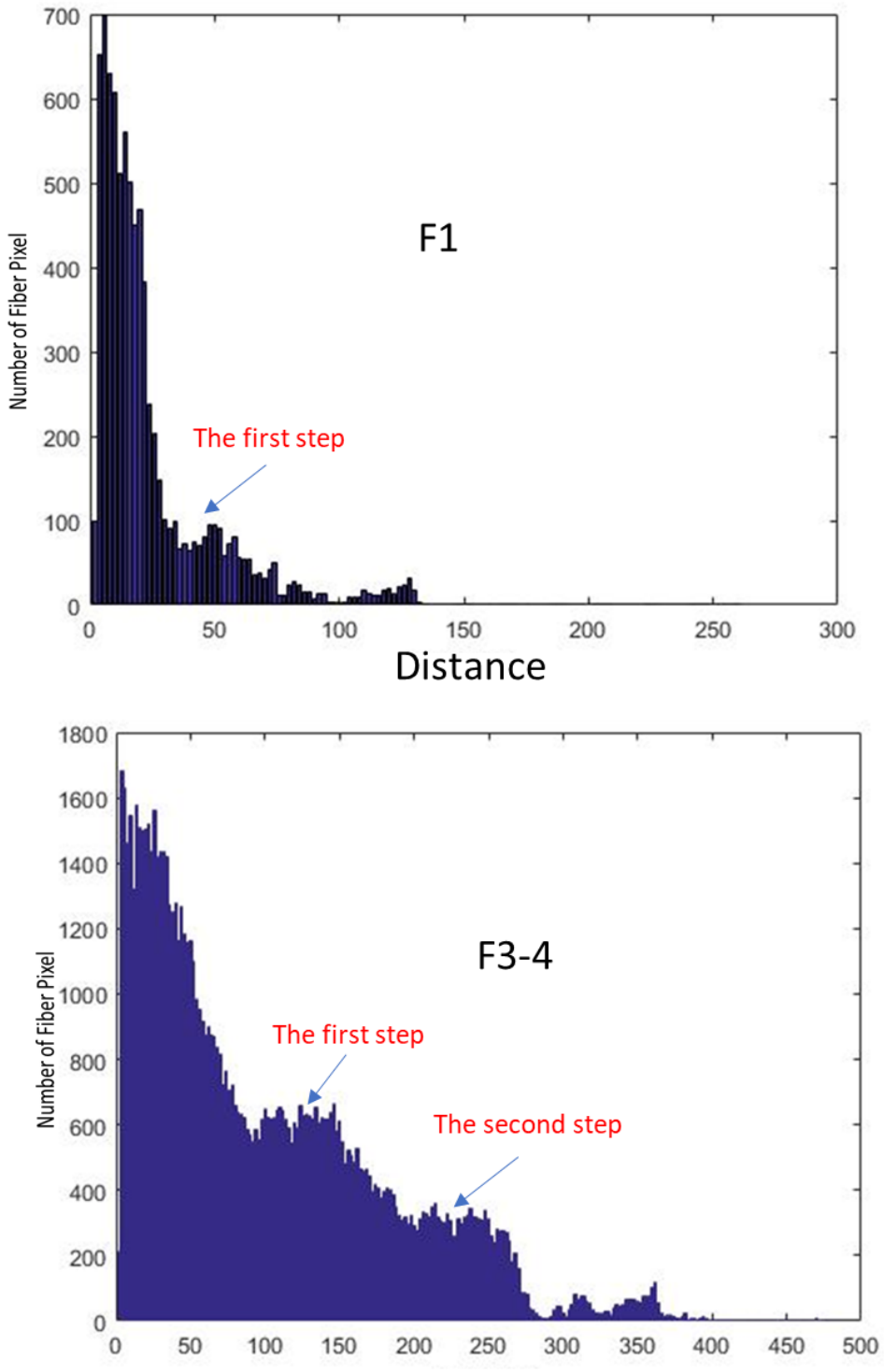

Figure 4-5 The number of fiber pixels vs. distance. The distance is an amount of space between the fiber pixels and the vein in the slice image. Upper: The curve which has short

one step represents to F1 stage. Lower: The curve which has the first and second step represents to F3-4 stage.

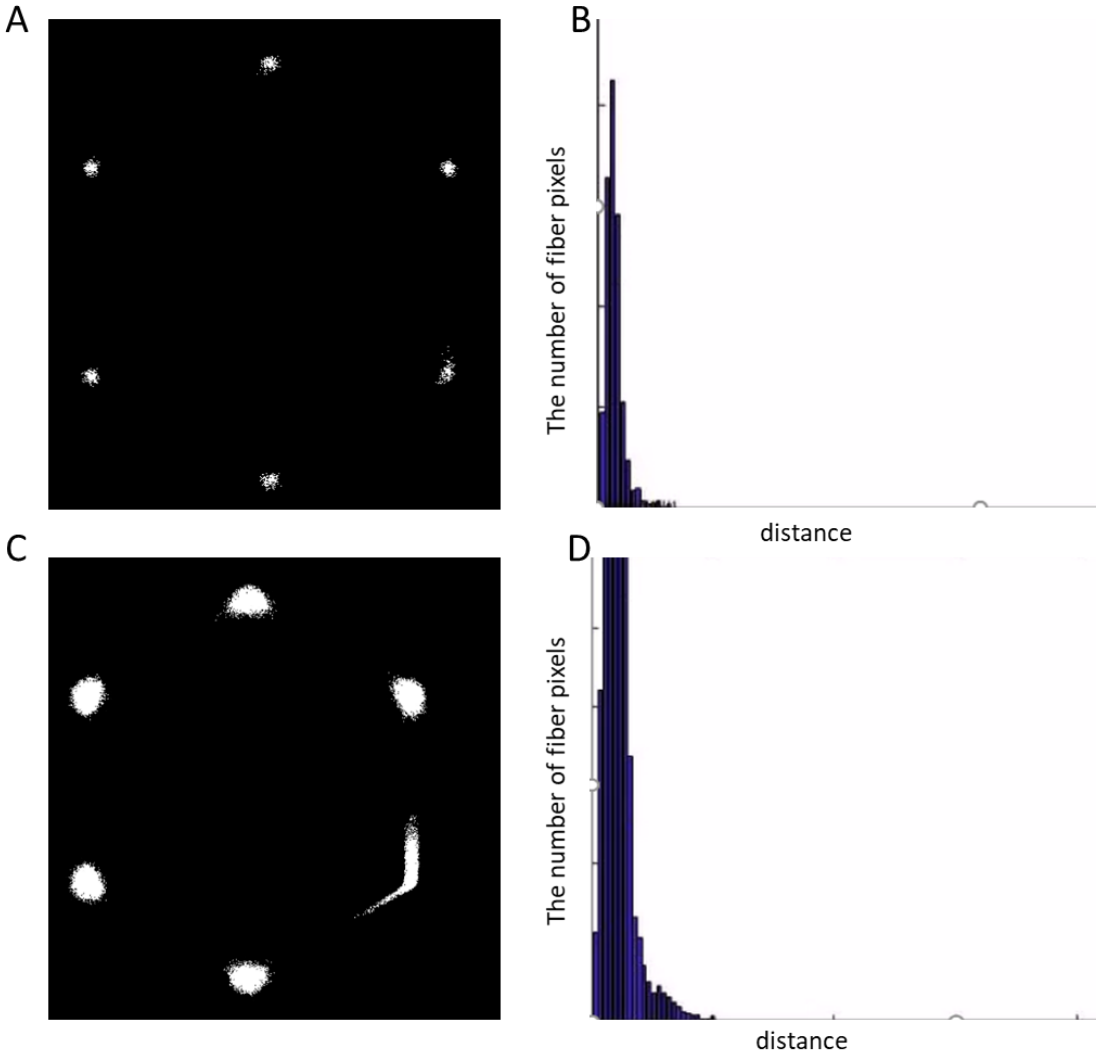

Figure 4-6 The simulation results. A and B are fiber growth in the single lobule. White is fiber. B and D is the number of fiber pixel vs. distance which are corresponding to A and B. A and C are F1 stage. B and D are the F2 stages.

We set the number of fiber pixels arrays of each tissue slide as the input data for machine learning. Each image was divided into four pieces; each piece has the same pathology and was resized to a standard size of 15000×15000 pixels to allow for automated image conversion. Then the model calculates all the distance between the fiber pixel and its nearest vessel.

Because of the large number of calculations, we used KdTree to improve the ability to find the location of the most adjacent vein. For machine learning, several methods, including Random Forest, the Nearest Neighbors, One vs. The Rest, Naïve Bays, and Support Vector Machine were used for training and testing purposes. The Random Forest was made by 30 trees, and the Nearest Neighbors set 15 neighbors in the model. The input has the stage and the number of pixels arrays. The final output contains possibility and outcomes corresponding to the liver fibrosis stage from F1 to F4. To compare the Performance of the features, we test the five machine learning algorithms based on the same liver slide images extracted. In the Random Forest model, we set 30 trees. In the Nearest Neighbors model, the number of neighbors is 15. In the Naïve Bayes, the alpha is 1, and binarize is 0.

We first evaluated the proposed methodology using the original 123 liver slides images obtained from different patients with liver fibrosis or cirrhosis. We set these slides into 3 groups, including F1 vs. F2-F4, F1-2 vs. F3-4 and F1-3 vs. F4. After training the features, the cross-validated performances of each machine learning model are shown in table 4.4-1.

Table 4.3-1 The cross-validation value for each stage with different machine learning models (n= 123).

	≥F2	≥F3	F4
Random Forest Classifier	0.39	0.32	0.29
Support Vector Machine	0.45	0.45	0.45
One-vs-The-Rest	0.39	0.32	0.32
Nearest Neighbors	0.33	0.33	0.33
Naïve Bayes	0.2	0.2	0.2

The results show low significance for the methodology in all five machine learning algorithms since the number of training images is not large enough. For more training samples, we cut the images into 4 pieces (Figure 4.6), to increase the number of training data. These pieces

have the same pathology report. The same features are extracted from the 492 images using previous methods. The size of each number array of features is 700. The cross-validated performances for the cut images are shown in table 4.4-2, the area under the ROC curve (AUC) values are in table 4.4-3.

Table 4.3-2 The cross-validation value for each stage with different machine learning models. The number of images is 492.

	≥F2	≥F3	F4
Random Forest Classifier	0.94	0.68	0.83
Support Vector Machine	0.9	0.57	0.83
One Vs The Rest	0.82	0.53	0.69
Nearest Neighbors	0.9	0.68	0.82
Naïve Bayes	0.71	0.57	0.67

Table 4.3-3 The AUC for each stage with different machine learning models.

	≥F2	≥F3	F4
Random Forest Classifier	0.972	0.736	0.842
Support Vector Machine	0.947	0.736	0.842
One Vs The Rest	0.608	0.467	0.6
Nearest Neighbors	0.972	0.625	0.842
Naïve Bayes	0.694	0.313	0.583

The new results have high cross-validation accuracies in each machine learning model, especially for the Random Forest model, Support Vector Machine, and Nearest Neighbors model. The AUC values show that the Random Forest model, support Vector, and Nearest Neighbors model all have good accuracy predicting stage. The Random Forest model has the highest value in each stage, so we select the Random Forest model to be the predicting model (figure 4-7).

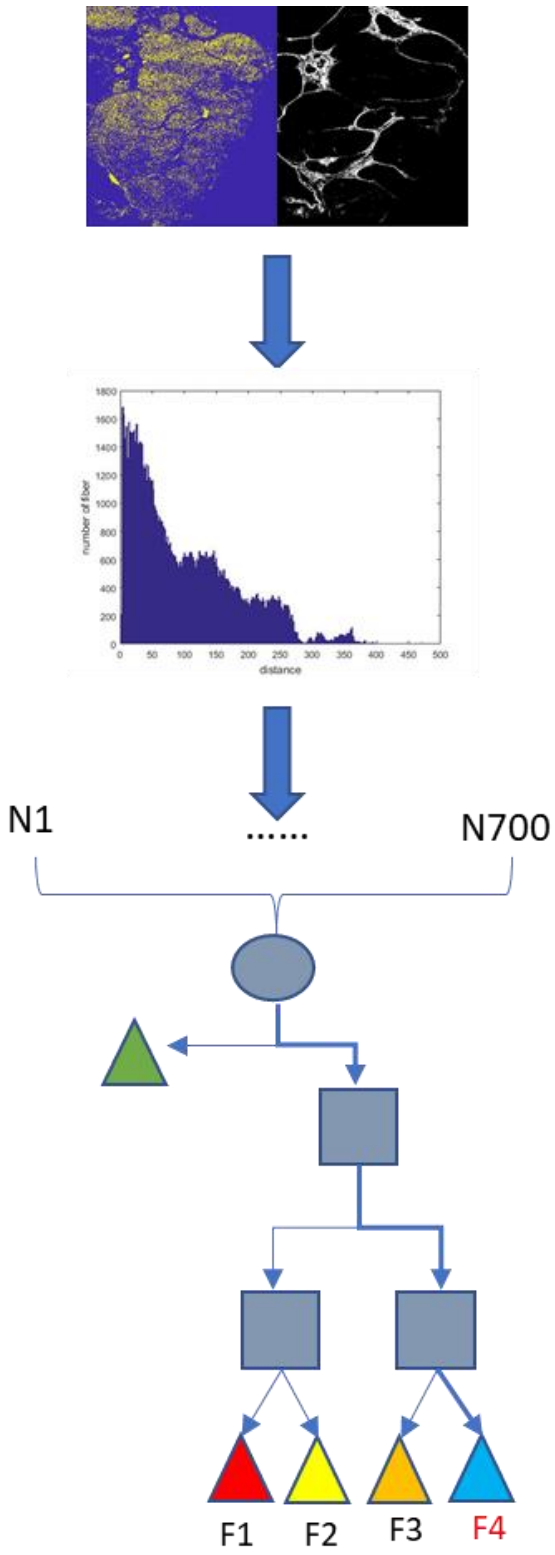

Figure 4-7 Random Forest for stratifying fibrosis stage. The numerical features which were derived from slices images act training features for random forest algorithm.

We build a fully automated methodology for grading liver fibrosis from liver slides. The Random Forest model has high cross-validation values, and AUC value was used to grade liver fibrosis. The new samples were classified by three predicting models, which indicate ≥F2, ≥F3, and F4. The first model prediction agrees with two grading results, ranging in [1:2] with a value of 1 labeling the fibrosis stage < F2, and a value of 2 for stages at F2-4 (Table 4.4-4).

Table 4.3-4 The predicting value for classification combinations. F1 is [1 1 1], F2 is [2 1 1], F3 is [2 2 1] and F4 is [2 2 2].

	≥F2	≥F3	F4
F1	1	1	1
F2	2	1	1
F3	2	2	1
F4	2	2	2

4.4 Discussions

In this chapter, we report a new, fully automated algorithm for fibrosis staging using slides stained with H&E and Masson. The numerical parameters derived from tissue images represent key features from METAVIR systems, such as portal fibrosis and fiber bundles. Our results show that the method can clearly distinguish between F1 and F3. The auto-grading methodology can score different patterns of fibrosis. Comparing with the deep learning algorithm, this method using machine learning decrease the number of training images under the supervision. Since the input is numerical parameters, the calculation of power required was reduced. CPU is up to this job. Meanwhile, the calculating/training time per each image for the standard reference is less than 15 mins. Analyzing each liver slides images uses only 15 seconds. These advantages can lay a foundation for application, which is auto-grading liver fibrosis.

The methodology successfully grades the liver fibrosis with high accuracy. The proposed method is designed to avoid the error from human interaction and manual work. Comparing with

different machine learning algorithms, we demonstrate that a machine learning-based algorithm using the numerical features-Random Forest model scores best. This machine-learning assisted, fully automated quantification of liver fibrosis grading, is a candidate for high-performance classification systems to examine liver slides.

5 THE DYNAMICS OF BLOOD FLOW IN LIVER

Liver fibrosis has a strong correlation with other diseases, such as diabetes and cancer [105]. Over the past two decades, the understanding of physiology and pathophysiology in liver fibrosis, especially early diagnosis of liver fibrosis has played a significant role in has improved the quality of life for cirrhotic patients [106]. Currently, techniques being explored for diagnose liver fibrosis are categorized as mainly the invasive and noninvasive measurements.

5.1 Existing liver fibrosis measurements

Liver biopsy, as an invasive method, is still treated as the gold standard for diagnosing hepatic fibrosis. However, it has a number of problems. The accuracy of liver biopsy is only 65% - 75% when biopsies are between 15mm and 25mm in length [1]. The invasive procedure is a high risk of operation in some pathophysiology, such as liver cancer, and required the patients to suffer the pain [2]. On the other hand, current noninvasive methods, such as transient elastography, are not very sensitive because of instrument accuracy and the subjectivity of operators.

Transient elastography (TE), as a proven technology of noninvasive procedure, uses the ultrasound wave to test the stiffness of the liver [107]. However, it is still limited by sample errors, instrument accuracy, and the subjectivity of operators. Because the liver is a large organ and deep in the body, other tissues and organs may affect the activity of ultrasound to render the profibrogenic grading [108]. The ultrasound wave of transient elastography only measures one point of the liver to measure the stiffness value.

We developed a new two-dimensional (2D) blood wave ultra-graphy (BDW) as a non-invasive technology to measure liver fibrosis. It constructs a new relationship between the dynamics of blood flow and the mechanical properties of the liver tissue, since the mechanical property of the liver is modified by the growing fiber network[108]. Compared with TE, it is not

limited by the size of the detection zone. Blood flows through the whole liver and carries the overall information of liver fibrosis. There are a few studies that applied the dynamics of blood on ultrasound images for liver fibrosis diagnosis, all of these studies found that cirrhosis can affect the blood flow and the velocity decrease.[109-112].

The stiffness of liver can be observed clearly sometimes, especially for late stage fibrosis, which is a valid bedside diagnosis for cirrhosis. Many studies have proven that the mechanical property of the liver is modified by the growth fiber network [113].

In the past decades, the research found that liver disease could affect the hepatic blood flow [114, 115]. The velocity of blood generally decreases with liver fibrosis progression [116]. However, there is no model nor data to accurately describe the dynamics of hepatic blood flow relative to liver fibrosis progression. In this chapter, we aim to develop a mathematical model that connects hepatic blood flow and liver fibrosis and use clinical data to support our model predictions.

5.2 Design and Model

The blood entre the liver mainly through portal veins, travels through the liver, and then exit the liver from the hepatic vein. As liver fibrosis progresses, the increased stiffness of the liver affects blood flow in the portal vein {references}. The effect in the vessel comes from the fiber structure and the mechanism of blood flow in the vein. The vascular wall was constructed by three parts, including intima, media, and adventitia (Figure 5-1). The intima of vein is endothelial cells tissue and elastic internal, responsible for building the smooth inter-surface and provide a protective screen between tissue and blood. The media are constructed by smooth muscle cells to maintain an elastic vascular wall. The adventitia consists of fibroblast, which when activated produce and deposit fibers.

Based on the property of the muscle pump, smooth muscle contraction provides the primary motive power of flood flow in the vein. This muscle involves standing swell and contract, help to bring venous blood. The structure of the cross-section of the vein has elastica interna, smooth muscle cells, and fibroblasts.

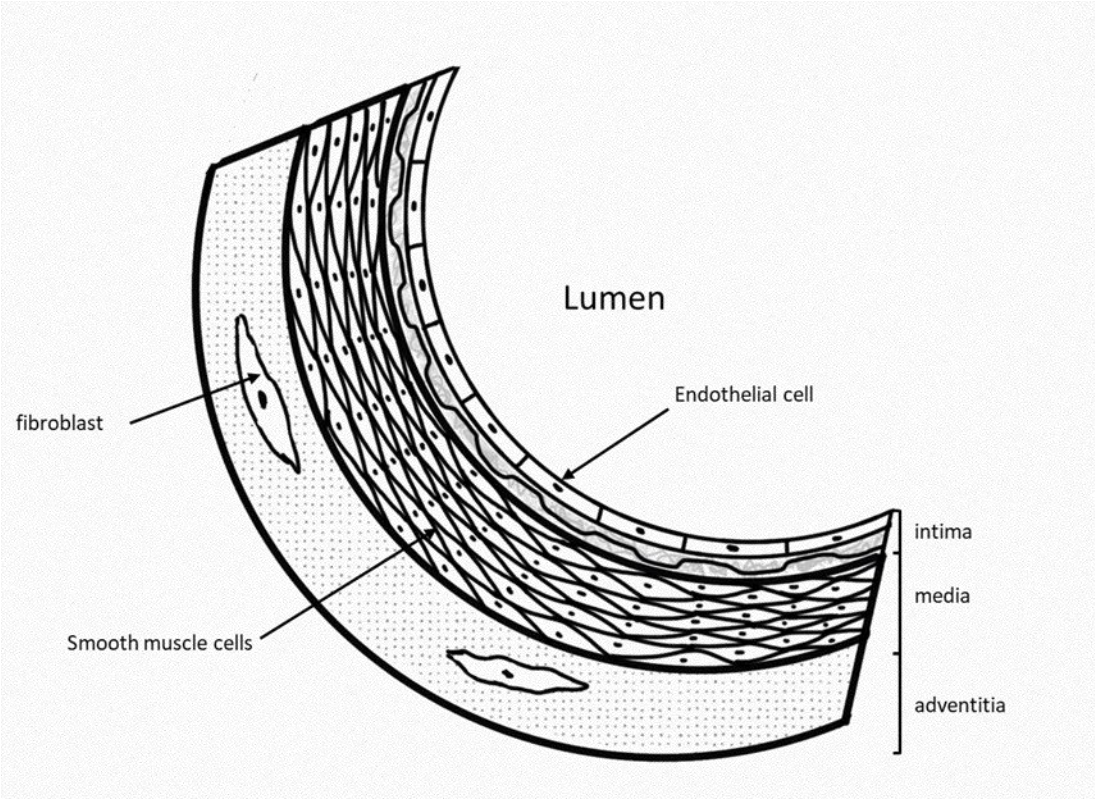

Figure 5-1 The structure of Vein. The intima of the vein is endothelial cells tissue and elastica interna. The media is smooth muscle cells, which is homogeneous tissue. The fibroblast locates in the adventitia.

We developed a physical model, which construct a novel relationship between the dynamics of blood flow and the mechanical properties of the liver tissue. The algorithms are designed to analyze the ultrasound Doppler images from hepatic patients. These results support the hypothesis of the model and suggest the possibility of using the dynamics of blood to identify a new noninvasive diagnostic tool for liver fibrosis.

In a chronically injured site in the liver, myofibroblasts generate and release the fibers at the adventitia. In other words, a skeletal fiber network encloses the vein and weaken the smooth muscle swelling when the blood presses the intima of the vein. The elasticity of the vein was damaged with the deposition of fiber.

When we assume elasticity of smooth muscle cells, the expansion and contraction of the vessel to pump blood flow can be modeled as a harmonic oscillator. We label the lowest velocity of blood at A point and the highest velocity of blood at B point (Figure 5-2).

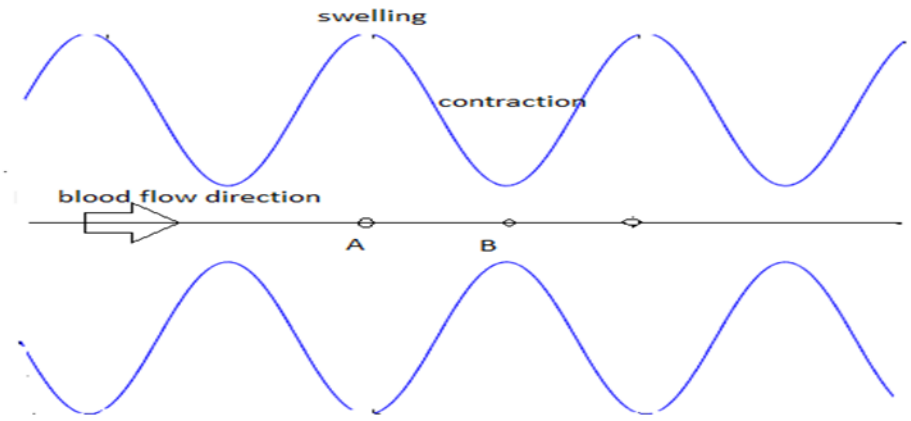

Figure 5-2 Illustration of blood flow in hepatic veins as driven by the elastic smooth muscle cells. The velocity of blood at A point is the lowest. The vessel is swelling. The velocity of blood at B point is the highest. The vessel is under contraction.

Each point on the wall of the vein keeps oscillating under the periodic contraction of the smooth muscle cells. Ignoring the damping effect of reducing energy, the equation of motion for each point along the vessel wall is described as

$$m\ddot{x} + kx = 0,$$

where m is mass of each point, k is the elastic coefficient of the smooth muscle, and x is the displacement of each point. Solving the motion equation, we have

$$x(t) = Acos(\omega t + \varphi)$$

where the angular velocity is related to the elastic coefficient of the vessel wall:

$$\omega = \sqrt{\frac{k}{m}}$$

In a fibrotic liver, when the fiber network encapsulates the vein, the elastic coefficient of the vessel wall increasing. In Chapter 2 we have introduced the mechanism of fiber response with liver fibrosis. $k_{fibrosis}$ is the elastic coefficient of the vascular wall under the fiber encapsulation. Because the fiber encapsulation increase the stiffness of vascular wall, $k_{fibrosis} > k$, we expect that

$$\omega_{fibrosis} = \sqrt{\frac{k_{fibrosis}}{m}} ,$$

the vessel oscillation frequency is higher in fibrotic liver than in healthy liver. Also, in the veins the velocity of blood is driven by the oscillation of vessel walls, we predict that the oscillatory features in blood flow in the veins also correlates with the stiffness of the vascular wall. Furthermore, because the blood entering portal veins, exiting through the hepatic vein, we expect that the difference of the blood flow between the portal vein and hepatic vein may reflect the degree of liver fibrosis.

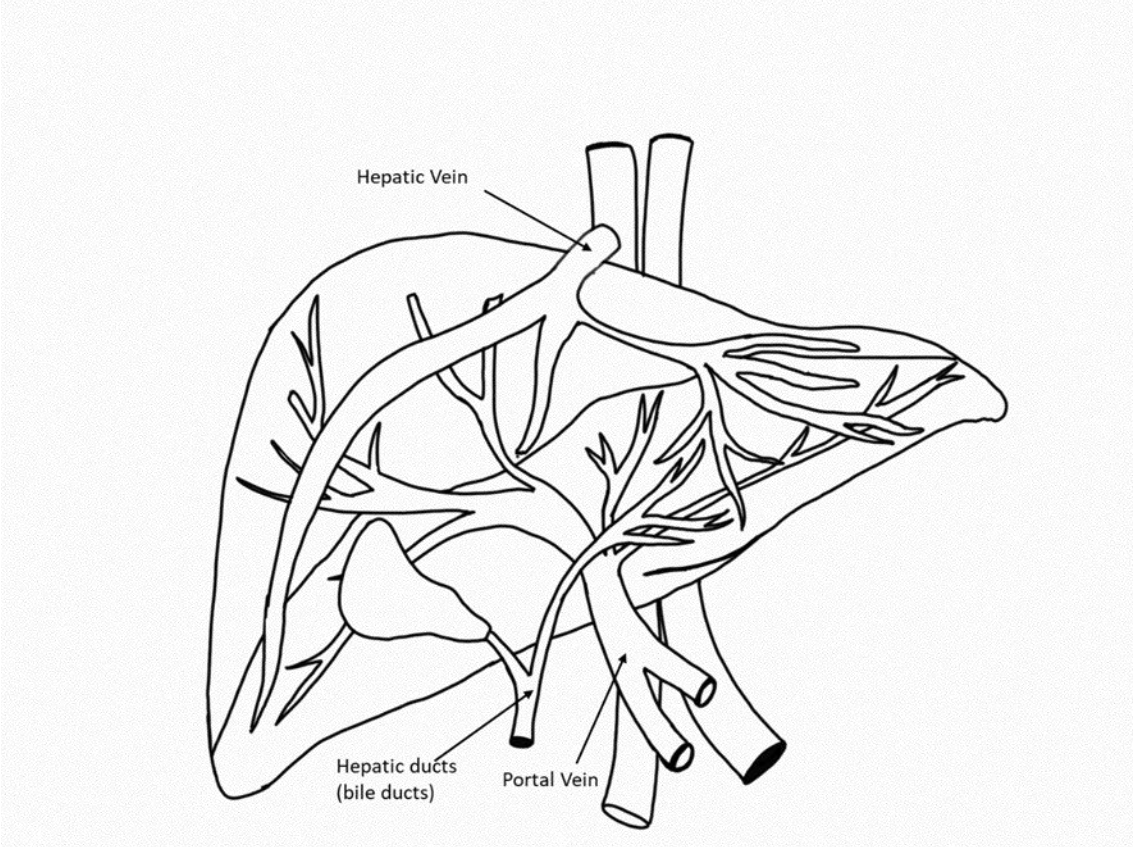

Figure 5-3 Vein structure in the liver. In the liver, the blood flow from the portal vein into the liver and flow out from hepatic vein.

To prove this predicted correlation, we measured the blood flow through ultrasound Doppler from the portal vein and hepatic vein, respectively (Figure 5-4).

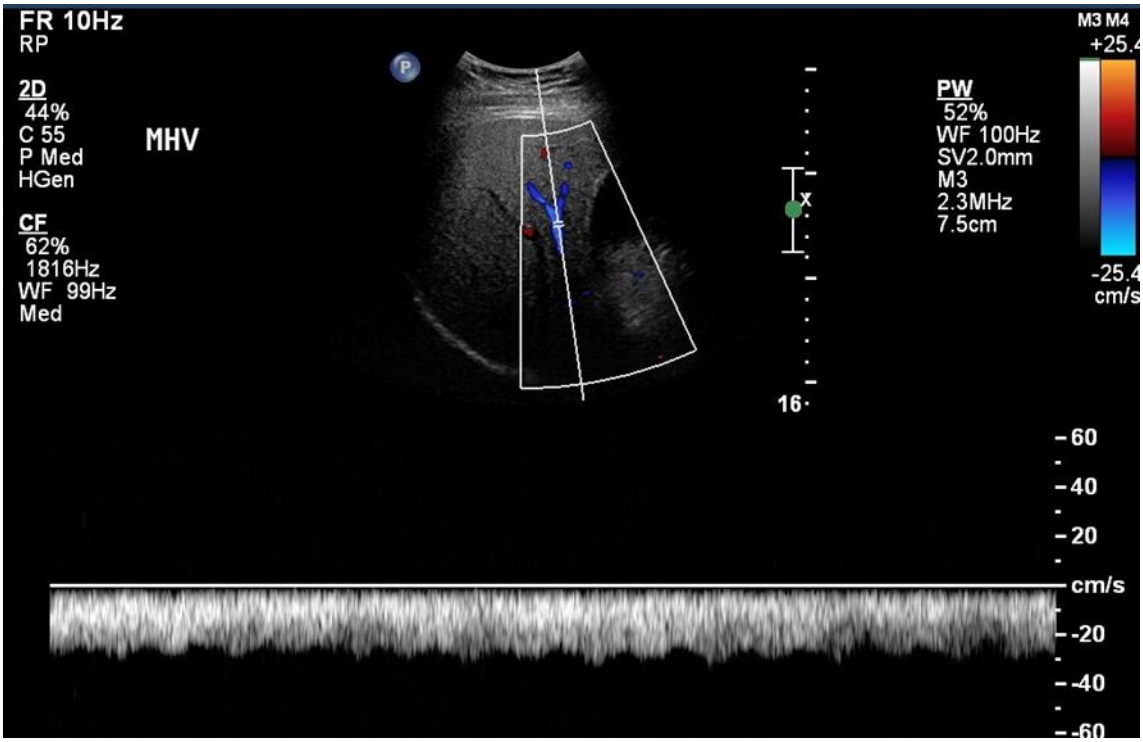

Figure 5-4 The ultrasound image with blood flow in middle hepatic vein. The image from Shijiazhuang fifth hospital.

Ultrasound Doppler imaging uses the high-frequency sound wave to view the blood flow in the liver. Since ultrasound Doppler is captured in real-time, the imagery could show the transformation of the velocity of blood with time. The wave pattern of blood was detached from the ultrasound image and leave the boundary of the pattern as the wave curve (Figure 5-5).

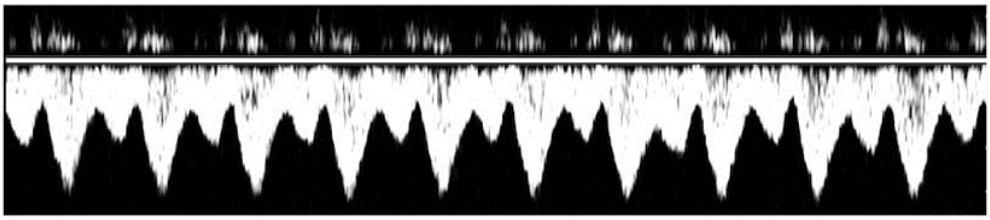

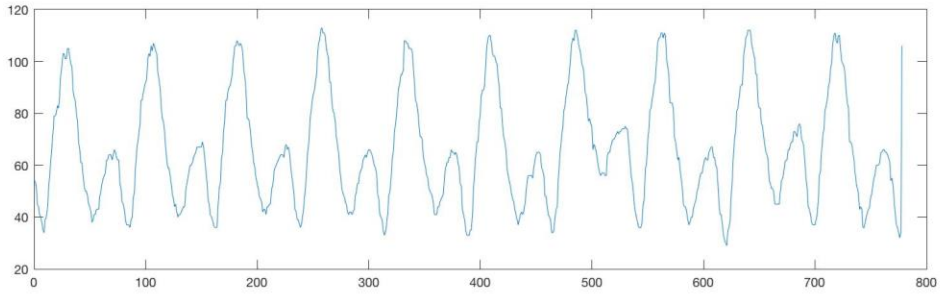

Figure 5-5 Upper: ultrasound image for blood flow. Lower: The boundary of the wave pattern. The ultrasound wave pattern was detected from human liver and describe the blood flow in the hepatic vein.

We selected four locations in the veins in the liver to measure the ultrasound Doppler images, including the entrance of the portal vein (PV), and the exit of the left (LHV), middle (MHV), and right hepatic vein (RHV), respectively. Then the Doppler signals, which measure the velocity of blood flow, were segmented from the ultrasound image. Since our model predicts that frequency is the signature parameter, we Fourier transform the time signals to the frequency domain, $\tilde{f}(\xi) = \int_{-\infty}^{\infty} f(t)\, e^{-2\pi i t \xi}\, dt$, where ξ is frequency and t is time (Figure 5-6)

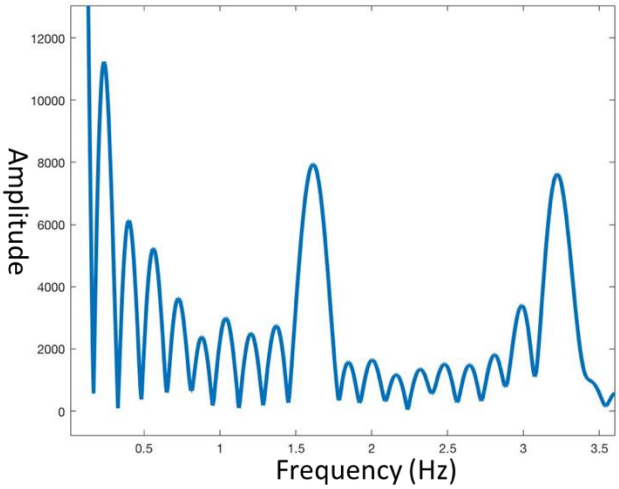

Figure 5-6 The Fourier transformed wave pattern of a typical Doppler signal in the frequency domain.

The wave pattern actually includes most of the effects we are looking at in blood flow dynamics, so the peak values in a frequency domain plot, though similar to the frequencies of heart beating, vary and carry information of fiber modification to blood flow. Comparing the selected peak value from the entrance and exit ultrasound images, the difference of each value will yield the response to the pathology (Figure 5-7).

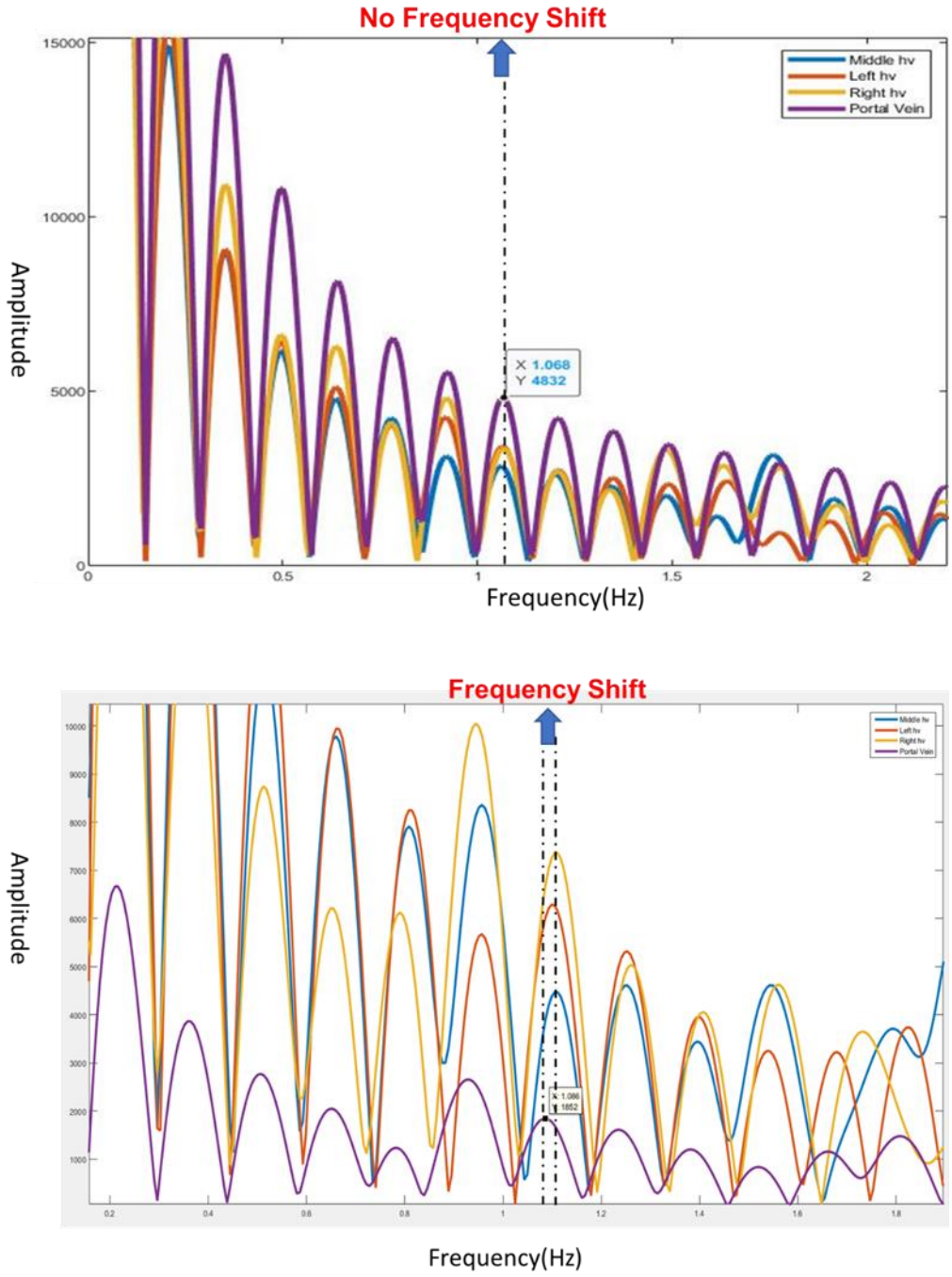

Figure 5-7 Comparing each frequency pattern from a different vein in the liver. Upper: No frequency shift at F0 between portal vein and hepatic veins. Lower: Frequency shift between portal vein and hepatic veins.

5.3 Material

5.3.1 Clinical data

Between Jun 2016 and October 2018, we performed ultrasound Doppler tests on 160 patients in two hospitals. The age and gender information of 160 patients was summarized in table 5.3-1. All test protocols followed the ethics guidelines and was approved by the ethics committee at the Zhongshan Hospital in Shanghai, and the Shijiazhuang Fifth Hospital in Shijiazhuang, China.

Table 5.3-1 Characteristics of patients with liver fibrosis.

	Age (%)		Sex (%)
Mean	43.377	Total	160
0-30	23.75%(38)	Male	65.63%(105)
31-40	20.00%(32)	Female	34.37%(55)
41-50	21.88%(35)		
51-60	20.00%(32)		
>60	14.38%(23)		

5.3.2 Blood wave ultra-graphy

Ultrasound doppler signals were obtained by the Doppler US imaging machine (Philips, GE). For independent ultrasound, images were detected at the portal vein, left hepatic vein, middle hepatic vein, and right hepatic vein from each patient (Figure 5-3). The time of detecting blood flow for each image is 6.6 seconds, during which patients need to hold breath.

Four independent ultrasound images and the heartbeat were obtained from each patient. To control quality through the entire procedure, operators who have more than ten years of ultrasound experience were enrolled in this study. Any ultrasound images were considered as unqualified when no signal or little valuable pattern was obtained in the ultrasound machine.

5.3.3 Liver biopsy

Liver biopsies were also taken from the same patients within four days of the ultrasound measurement, providing the gold standard for grading of liver fibrosis. Each biopsy was stained with Masson's trichrome. Grading of all the biopsy was based on the METAVIR scoring system. The biopsy samples with sizes smaller than 15mm or failed stain, were excluded.

5.3.4 Serological examinations

All serological examinations were measured within four days of ultrasound detection. The white blood cell, hemoglobin (HGB), platelet (PLT), alanine aminotransferase (ALT), aspartate aminotransferase (AST), gamma-glutamyl transpeptidase (GGT), albumin (ALB), globulin (GLB), bilirubin (DBIL), blood ureanitrogen (BUN), serum creatinine (sCr), prothrombin time (PT), international normalized ration (INR) were recorded. The FIB-4 as biomarker model was calculated as FIB-4 = [age (year)] × [AST (U/L)]/[platelet count (109/L) × ALT (U/L)1/2][11].

5.3.5 Blood flow model in ultrasound image

Four ultrasound images were analyzed following three steps: feature detection, feature analysis, and computational prediction.

Doppler signals were cropped from ultrasound images, with a standard size of 800*1600 pixels. The envelop of the signals were extracted, and Fourier transformed. The frequency difference between the portal vein and the averaged frequency of the hepatic veins is the value that correlates to liver fibrosis score.

5.3.6 Statistical analysis

All the statistical data were summarized as mean±SD, median and interquartile range (IRQ). Student's t-test were applied to compare groups. Sensitivity, specificity, positive, and negative predicate values were calculated. The area under the receiver operating characteristic

(ROC) curve (AUC) is the evaluation metrics for checking the correctness in estimation of liver fibrosis stages. All data were tested between two groups, and the p-value of less than 0.01 indicated a significant correlation. The statistical analyses were conducted using R software.

5.4 Results

The serological examinations were summarized in Table 5.4-1. P-value was calculated between variables and the stage of liver biopsies.

Table 5.4-1 Baseline characters of patients.

Variables	mean ± SD	P-value
WBC	5.69±3.52	0.0204
PLT (10^9/L)	189.76±80.2	1.496e-11
ALT (IU/L)	71.31±76.47	0.5903
GGT (IU/L)	86.97±133.87	0.1636
ALB (g/L)	43.39±5.91	0.0006464
HGB (g/L)	137.78±23.57	0.06645
AST (IU/L)	53.04±66.12	0.9342
BUN	4.54±1.26	0.7284
sCr	63.97±13.74	0.7373
PT (%)	11.71±3.23	0.001399
INR	1±0.11	0.000238

Table 5.4-2 Performance of Blood Flow, FIB-4 for the assessment of liver fibrosis stages.

Cirrhosis	AUC	Sensitivity	Specificity
BDW	0.9473	0.8919 (0.9730-0.7838)	0.9333 (0.9750-0.8833)
FIB-4	0.777	0.8378 (0.7027-0.9459)	0.6417 (0.5583-0.7027)
PL	0.7377	0.8297 (0.8649-0.5676)	0.5917 (0.6833-0.5000)
PM	0.8001	0.7297 (0.8649-0.5946)	0.8417 (0.9000-0.7750)
PR	0.7423	0.6757 (0.8378-0.5135)	0.8083 (0.8750-0.7333)
PLM	0.8967	0.8378 (0.9459-0.7027)	0.9500 (0.9833-0.9083)
PLR	0.8277	0.8108 (0.9189-0.6757)	0.8000 (0.8667-0.7250)
PMR	0.8837	0.8378 (0.9459-0.7027)	0.9000 (0.9500-0.8417)

≥F3	AUC	Sensitivity	Specificity
BDW	0.9425	0.9107 (0.9821-0.8214)	0.8614 (0.9208-0.7921)
FIB-4	0.7917	0.8036 (0.8929-0.6964)	0.5545 (0.6436-0.4554)
PL	0.7051	0.6607 (0.7857-0.5357)	0.6139 (0.7030-0.5248)
PM	0.7486	0.7500 (0.8571-0.6429)	0.5743 (0.6733-0.4752)
PR	0.7728	0.6607 (0.7857-0.5357)	0.8812 (0.9406-0.8119)
PLM	0.8443	0.8036 (0.9107-0.6964)	0.6832 (0.7723-0.5941)
PLR	0.8548	0.8036 (0.8929-0.6964)	0.8713 (0.9307-0.8020)
PMR	0.8815	0.8393 (0.9286-0.7321)	0.8416 (0.9109-0.7723)

≥F2	AUC	Sensitivity	Specificity
BDW	0.9438	0.9048 (0.9643-0.8333)	0.7945 (0.8767-0.6986)
FIB-4	0.786	0.7262 (0.8214-0.6310)	0.6712 (0.7671-0.5616)
PL	0.7237	0.619 (0.7262-0.5119)	0.7397 (0.8356-0.6438)
PM	0.8076	0.7976 (0.8810-0.7143)	0.6849 (0.7945-0.5753)
PR	0.782	0.6429 (0.7384-0.5357)	0.8356 (0.9178-0.7534)
PLM	0.8658	0.8333 (0.9167-0.7500)	0.7397 (0.8356-0.6301)
PLR	0.8542	0.8333 (0.9048-0.7500)	0.7808 (0.7500-0.6712)
PMR	0.9048	0.8690 (0.9405-0.7976)	0.8356 (0.9045-0.7397)

*Statistical quantifications were demonstrated with 95% CI, when applicable.

*Sensitivity and Specificity include the lowest and highest value.

*BDW, blood flow (PV versus LHV, MHV, and RHV); FIB-4, fibrosis index based on four factors; PL, PV versus LHV; PM, PV versus MHV; PR, PV versus RHV; PLM, PV versus LHV and MHV; PLR, PV versus LHV and RHV; PMR, PV versus MHV and RHV.

In the results, BDW demonstrated the highest AUC, sensitivity, and specificity compared with all other methods for classifying cirrhosis, ≥F3, and F2 (Table 5.4-2 and Figure 5-8). All the AUCs were statistically significant (p-value <0.001). AUCs of BDW start from 0.9473, 0.9425, and 0.9438 for three stages, respectively, which were 0.1703, 0.1508, and 0.1578 higher than the AUCs of FIB-4. The sensitivity and specificity also have better Performance than FIB-4 and other analyses. PMR, which only analysis MHV and RHV, has the second-highest AUCs. In the three single hepatic veins, MHV and RHV were better than LHV. Since LHV is near the heart, the noise of the heart may affect the accuracy of LHV.

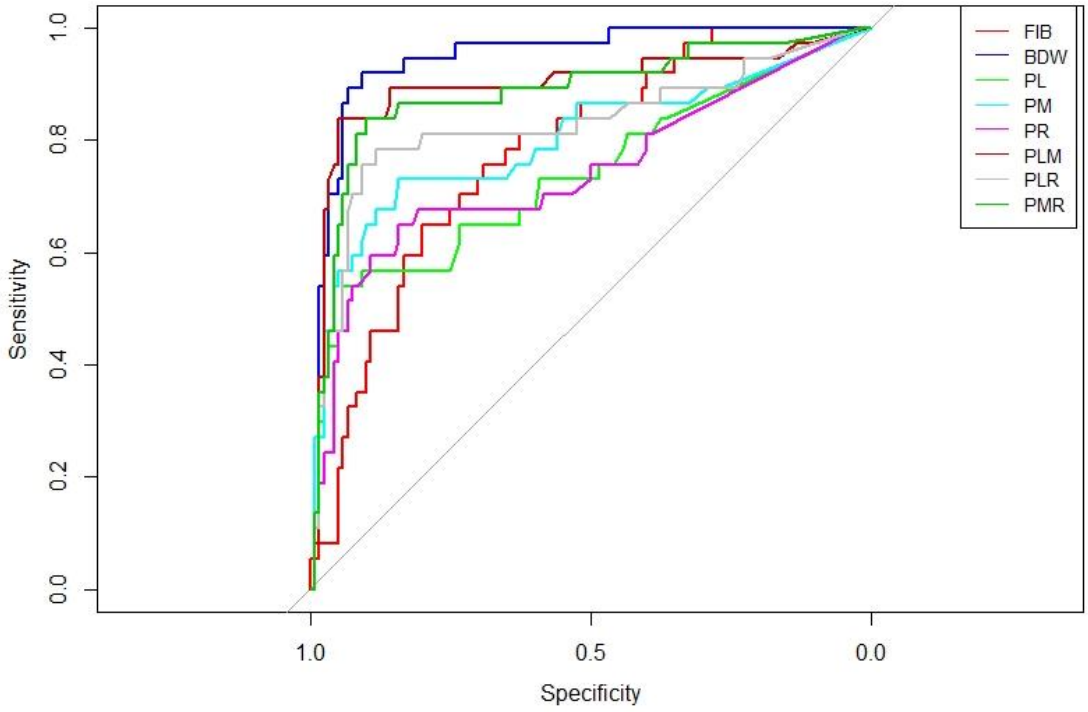
FIB
BDW
PL
PM
PR
PLM
PLR
PMR
Sensitivity
0.0
0.2
0.4
0.6
0.8
1.0
1.0
0.5
0.0
Specificity

A

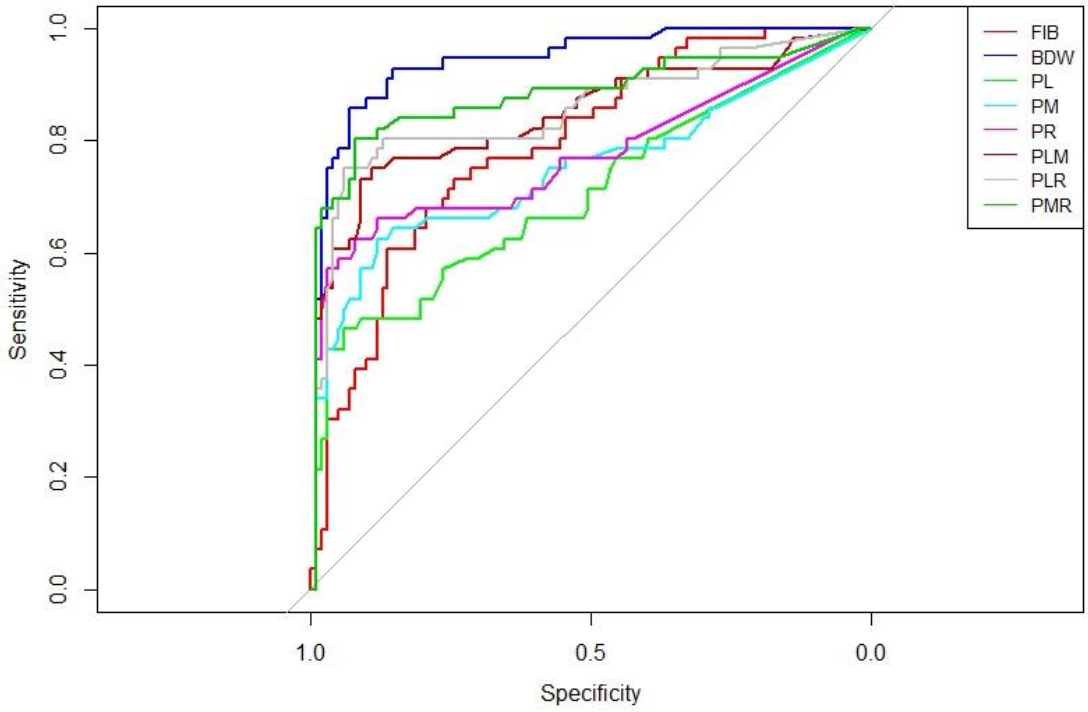
FIB
BDW
PL
PM
PR
PLM
PLR
PMR
Sensitivity
0.0
0.2
0.4
0.6
0.8
1.0
1.0
0.5
0.0
Specificity

B

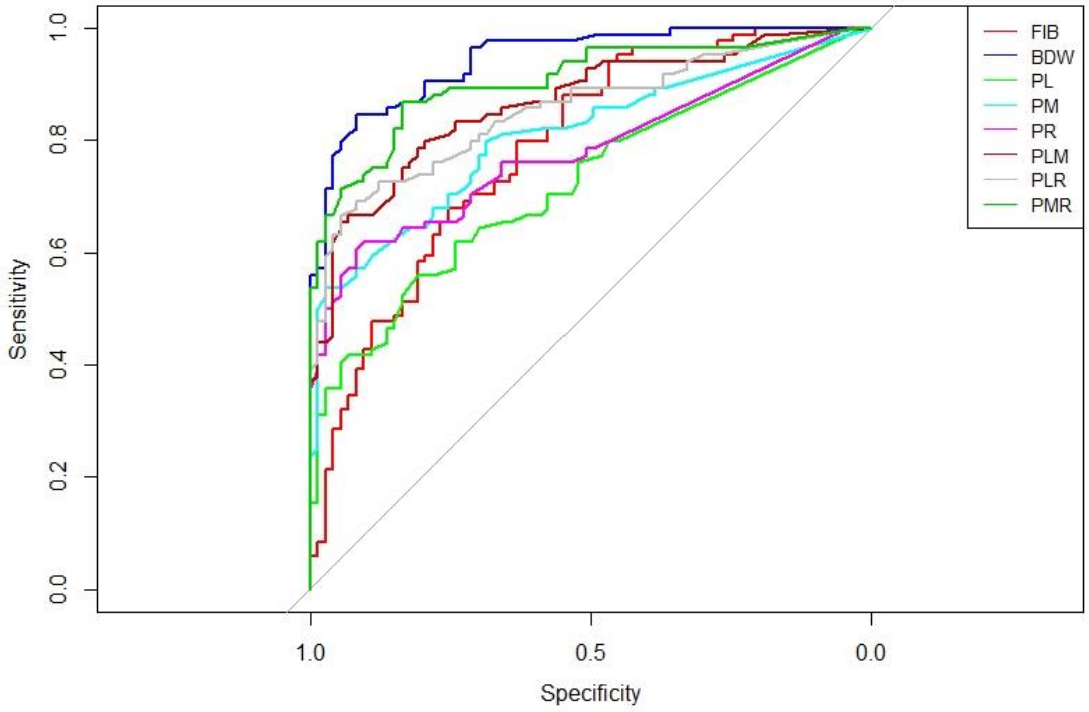

C

Figure 5-8 ROC curves with BDW, FIB-4, PL, PM, PR, PLM, PLR, and PMR for the assessment of liver fibrosis stages, respectively. A. The ROC of cirrhosis (F4). B. The ROC of advanced fibrosis (F0-F2 versus F3-4). C. The Roc of significant fibrosis (F0-F1 versus F2-F4).

To investigate if other confounding factors, such as age, gender, weight, and inflammation state would impact these results, we randomly selected three cohorts (n=120) from all the patients (n=160) to test correlation. For each fibrosis classification, the ROC of three cohorts always overlapped each other (Figure 5-9). The AUCs are not much different (Table 5.4-3). These results demonstrated that BDW has stable performance regardless of age and weight.

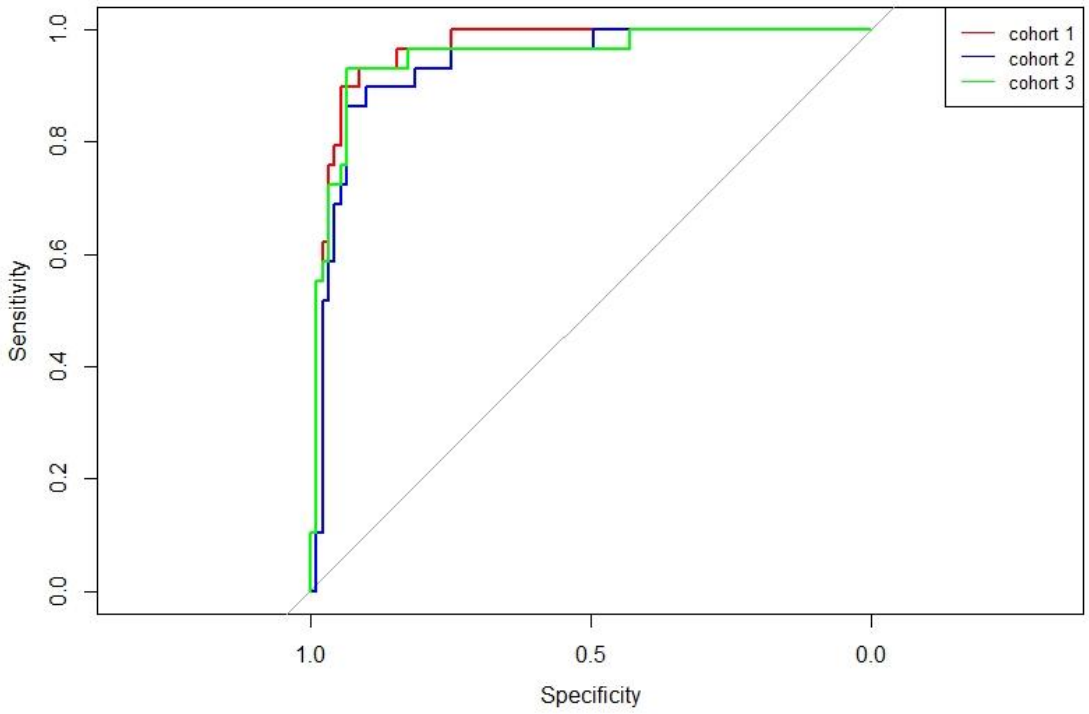
cohort 1
cohort 2
cohort 3
Sensitivity
0.0
0.2
0.4
0.6
0.8
1.0
1.0
0.5
0.0
Specificity

A

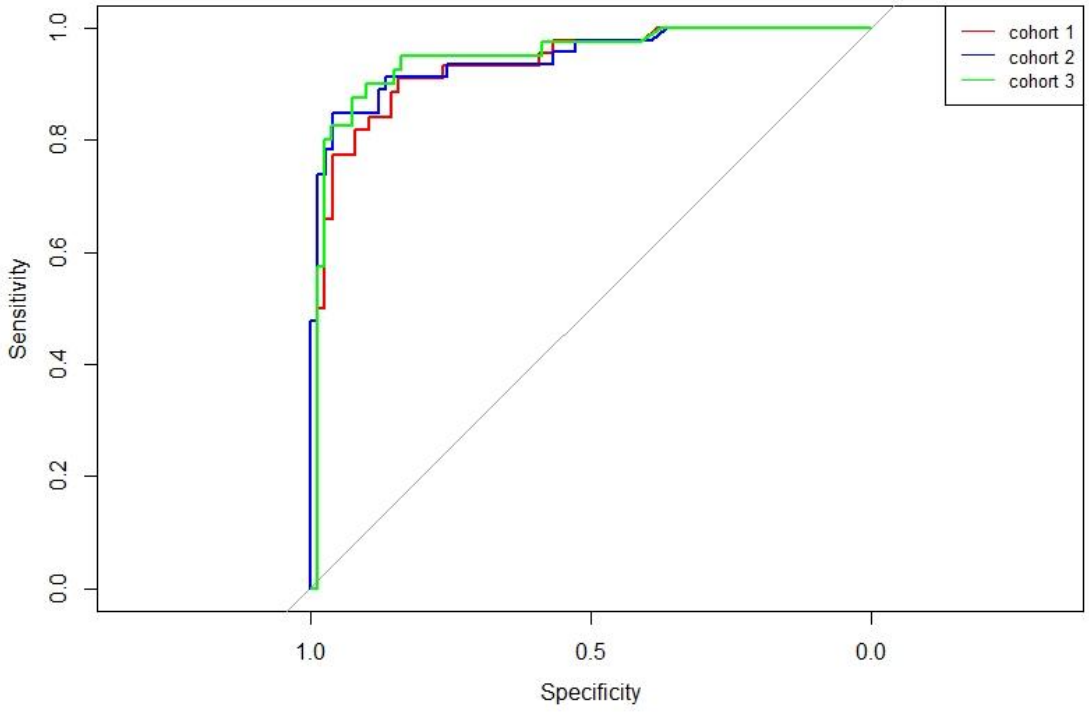
cohort 1
cohort 2
cohort 3
Sensitivity
0.0
0.2
0.4
0.6
0.8
1.0
1.0
0.5
0.0
Specificity

B

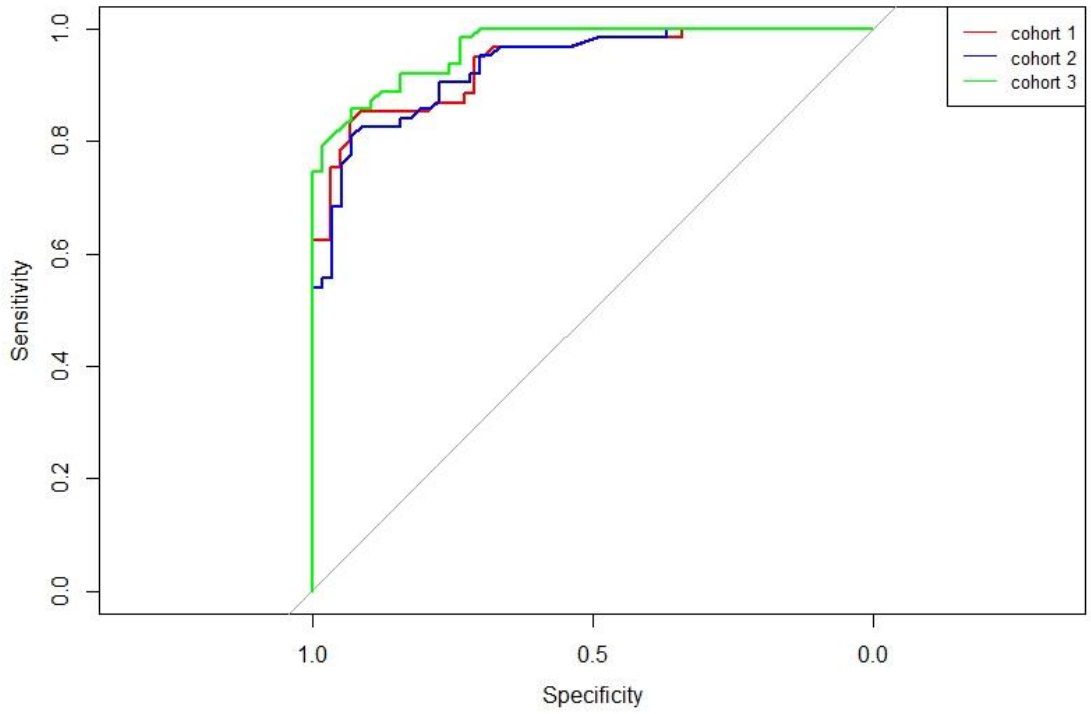

C

Figure 5-9 ROC curves with cohort 1, cohort 2, and cohort 3 for the assessment of liver fibrosis stages, respectively. A. The ROC of cirrhosis (F4). B. The ROC of advanced fibrosis (F0-F2 versus F3-4). C. The Roc of significant fibrosis (F0-F1 versus F2-F4). The number of patients are 120 in each cohort.

Table 5.4-3 Performance of cohort 1, cohort 2, and cohort 3 (n=???) for the assessment of liver fibrosis stages.

	AUC	Sensitivity	Specificity
Cirrhosis			
cohort 1	0.9474	0.9333 (0.8333-1.0000)	0.9444 (0.8889-0.9889)
cohort 2	0.9522	0.9259 (0.8148-1.0000)	0.9462 (0.9030-0.9892)

cohort 3	0.9453	0.9167 (0.7917-1.0000)	0.9375 (0.8854-0.9792)
≥F3			
cohort 1	0.9303	0.9091 (0.8182-0.9773)	0.8421 (0.7632-0.9211)
cohort 2	0.9459	0.9133 (0.8261-0.9783)	0.8649 (0.7838-0.9324)
cohort 3	0.9467	0.9000 (0.8000-0.9750)	0.9000 (0.8250-0.9625)
≥F4			
cohort 1	0.9387	0.9508 (0.8852-1.0000)	0.7119 (0.5932-0.8305)
cohort 2	0.9337	0.9048 (0.8254-0.9683)	0.7719 (0.6667-0.8772)
cohort 3	0.9664	0.9206 (0.8571-0.9841)	0.8421 (0.7368-0.9298)

For the three-strategy comparison, BDW showed similar performance. AUCs of BDW was significantly better than FIB-4 in all fibrosis stages. We compare BDW values and transient elastography results (Figure 5-10), and show that BDW distinguishes between healthy people and patients with early stage fibrosis is better than the transient elastography.

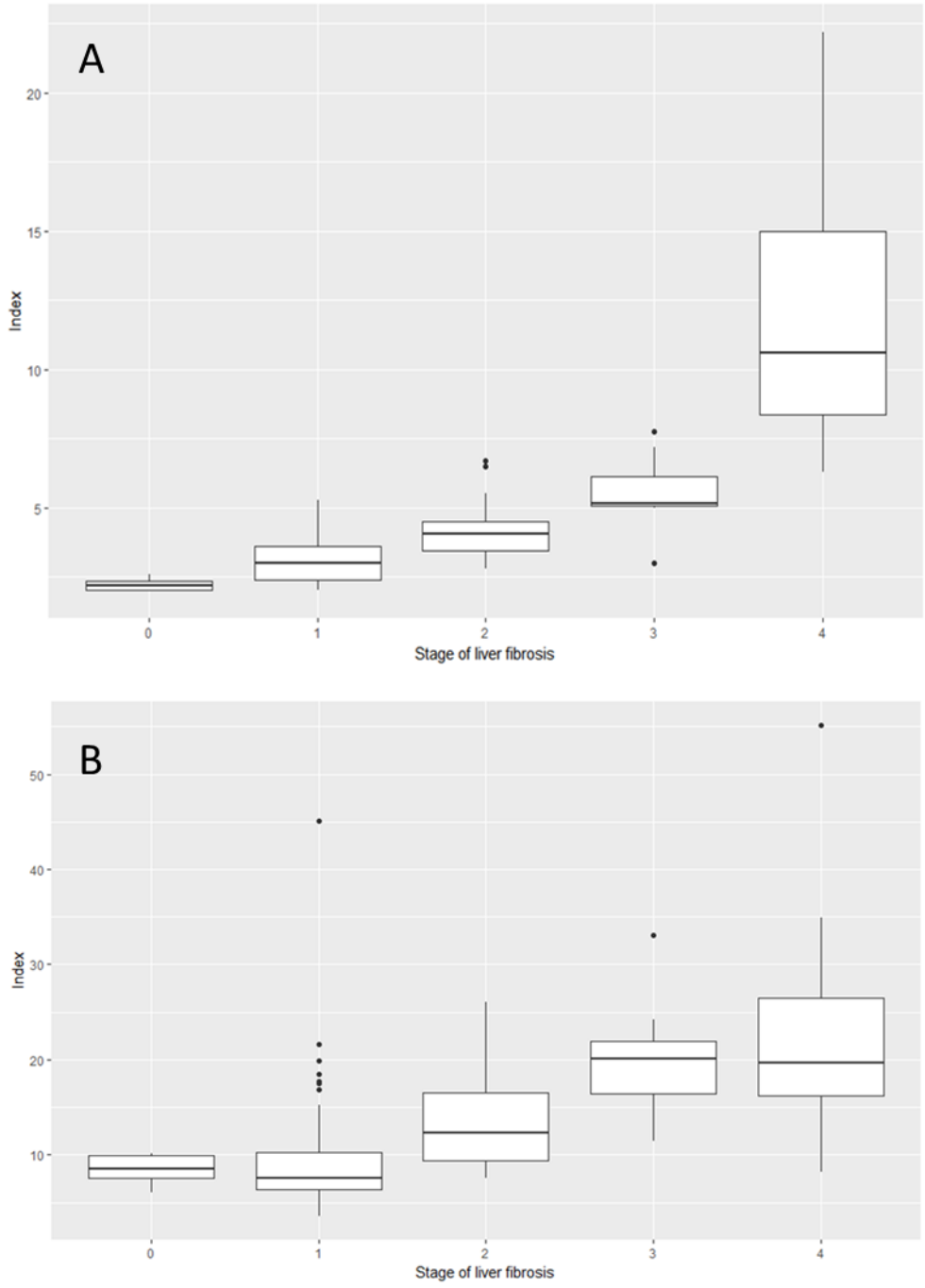

Figure 5-10 The values in liver fibrosis stages. A. The error bar shows the BDW versus the stage of liver fibrosis. B. The error bar shows the value of transient elastography versus the stage of liver fibrosis. CI is 95%.

5.5 Discussions

In this study, we developed a physical model to describe the dynamic of blood flow in the liver. The model improved the understanding of how the blood flows in the hepatic vein and how fibrosis affects the dynamics of blood flow. Based on this model, we measured the ultrasound Doppler images of PV, LHV, MHV, and RHV and calculated the frequency differences between the PV and the HVs as a measurement for liver fibrosis. For these data, the diagnostic accuracy of BDW was compared with FIB-4 and biopsy readings. In cirrhosis (F4), advanced fibrosis (>F3), and significant fibrosis, (>F2). BDW performed significant superiority against FIB-4 and others. BDW, with AUCs reaching 0.945, shows similar diagnostic accuracy compared to the reference standard liver biopsy. For assessing advanced fibrosis and significant fibrosis, PMR had the second-highest diagnostic accuracy, with AUCs were 0.8815 and 0.9048. In the cirrhosis, PLR showed the second-highest diagnostic accuracy with AUC of 0.8967. Comparing with three signal hepatic veins, LM had the highest AUC of 0.8007, 0.7486, and 0.8076, which did not show a significant difference in FIB-4 tests.

To investigate the influence of other factors, such as age, weight, and inflammation, we analyzed three cohorts in ROCs. These factors did not show a significant impact on the performance of BDW.

These results indicate that BDW can be used for the assessment of liver fibrosis and provides a high diagnostic accuracy in classifying liver fibrosis stages. This study is the first time to build a quantitative relationship between the hepatic blood flow and liver fibrosis, and demonstrates a novel non-invasive liver fibrosis diagnosis with high accuracy. However, the limitation of this study was the limited population size and the unbalanced stage distribution of the population. In further research, we will recruit more patients with both ultrasound measurements

and liver biopsy. We will also enroll patients of different chronic liver conditions, including HBV-infected and NASH Patients. In conclusion, BDW performed a high diagnostic accuracy and has a potential to apply for non-invasive liver fibrosis diagnosis.

6 Summary

The liver fibrosis can develop in patients with any type of chronic liver disease, including alcoholic liver disease, hepatitis C, hepatitis B, nonalcoholic fatty liver disease (NAFLD), and autoimmune hepatitis. Alcoholic liver disease is a leading cause of liver disease and liver-related deaths globally, particularly in developed nations. The Centers for Disease Control (CDC) estimates that 19,388 people died in the US from alcohol-related liver disease in 2014. Results of the 2015 National Survey on Drug Use and Health indicate that 15.1 million adults aging 18 and older struggle with alcohol use disorder. The CDC further estimates that approximately 3.2 million Americans are chronically infected with the hepatitis C virus, with an estimated 8,000 to 10,000 hepatitis C virus-related deaths annually. By far, the largest and fastest-growing population at risk for developing hepatic fibrosis are individuals with NAFLD, which is often associated with one or more aspects of metabolic syndrome. A significant number of people with NAFLD also have liver inflammation and fibrosis. This constellation of liver pathology is termed nonalcoholic steatohepatitis or NASH. GlobalData epidemiologists forecast that the total prevalence of NASH in the United States, the United Kingdom, France, Germany, Italy, Spain, and Japan will grow by an annual growth rate (AGR) of 0.64% per year over the next ten years, from 61,295,898 cases in 2016 to 65,201,742 cases in 2026. In the 7MM, the US will have the highest number of total prevalent cases throughout the forecast period, with 34,972,594 cases in 2016 and 38,256,918 cases in 2026.

The key to preventing liver fibrosis from advancing to more deadly diseases, including cirrhosis and liver cancer, is to diagnose and reverse fibrosis in its early stage. Early stages of fibrosis, however, are challenging to detect because they are asymptomatic. Too often, when liver disease is first diagnosed, it is too late to avoid potentially fatal outcomes. Furthermore, evaluation

of treatment-efficacy of interventions to halt or reverse liver disease relies on assessing the stage of fibrosis.

Existing technologies for fibrosis detection are 1) invasive, inaccurate, and risky (biopsy); or 2) noninvasive, expensive with severe shortcomings in terms of both accuracy and accessibility. To overcome these limitations and offer a more accurate non-invasive method for fibrosis detection, we conducted the following studies.

First, we developed a fiber-pixels model for liver fibrosis, describing the critical interaction between hepatocytes and the fiber. The fiber-pixels model also builds the 2D image to simulate the fiber patterns in various liver fibrosis stages. These images can be supplemental training samples in machine learning or deep learning models.

Second, we developed a new machine learning method to auto-stage liver fibrosis based on histopathological slides. Compared with other machine learning models, our numerical features-random forest model uses less than 15 seconds to analyze one biopsy image with clinical accuracy.

Third, we developed a physics-based model to connect blood flow dynamics and stages of liver fibrosis. Analysis on clinical data using Ultrasound Doppler measurements showed improvements compared with elastography and serologic measurements.

Last, this new noninvasive fibrosis detection methods shows good translational potential, as it improves upon the state-of-the-art by offering a more accurate, safer, and more convenient noninvasive method of detection. The potential users are doctors and clinicians, hospitals, and other healthcare providers, ultrasound manufactures, as well as pharmaceutical companies for evaluating liver fibrosis stage and progression.

REFERENCES

1. Czaja, A.J., *Hepatic inflammation and progressive liver fibrosis in chronic liver disease.* World journal of gastroenterology: WJG, 2014. **20**(10): p. 2515.
2. Scaglione, S., et al., *The epidemiology of cirrhosis in the United States.* Journal of clinical gastroenterology, 2015. **49**(8): p. 690-696.
3. Miele, L., et al., *Noninvasive assessment of fibrosis in non-alcoholic fatty liver disease (NAFLD) and non-alcoholic steatohepatitis (NASH).* Translational research, 2007. **149**(3): p. 114-125.
4. Bedossa, P., D. Dargère, and V. Paradis, *Sampling variability of liver fibrosis in chronic hepatitis C.* Hepatology, 2003. **38**(6): p. 1449-1457.
5. Kagan, H., *Lysyl oxidase: mechanism, regulation and relationship to liver fibrosis.* Pathology-Research and Practice, 1994. **190**(9-10): p. 910-919.
6. Takahara, T., et al., *Type VI collagen gene expression in experimental liver fibrosis: quantitation and spatial distribution of mRNAs, and immunodetection of the protein.* Liver, 1995. **15**(2): p. 78-86.
7. DEGOTT, C., et al., *Myeloid metaplasia, perisinusoidal fibrosis, and nodular regenerative hyperplasia of the liver.* Liver, 1985. **5**(5): p. 276-281.
8. Caturelli, E., et al., *Transcatheter arterial chemoembolization for hepatocellular carcinoma in patients with cirrhosis: evaluation of damage to nontumorous liver tissue—long-term prospective study.* Radiology, 2000. **215**(1): p. 123-128.
9. FRANKEL, J.J., C.E. ASBURY, and L.A. BAKER, *Hepatic insufficiency and cirrhosis in diabetes mellitus.* Archives of Internal Medicine, 1950. **86**(3): p. 376-390.
10. Sato, S., et al., *Clinical comparison of branched-chain amino acid (l-Leucine, l-Isoleucine, l-Valine) granules and oral nutrition for hepatic insufficiency in patients with decompensated liver cirrhosis (LIV–EN study).* Hepatology research, 2005. **31**(4): p. 232-240.
11. Bosch, J. and J.C. García-Pagán, *Complications of cirrhosis. I. Portal hypertension.* Journal of hepatology, 2000. **32**: p. 141-156.
12. De Franchis, R. and M. Primignani, *Natural history of portal hypertension in patients with cirrhosis.* Clinics in liver disease, 2001. **5**(3): p. 645-663.
13. Hutterer, F., M. Eisenstadt, and E. Rubin, *Turnover of hepatic collagen in reversible and irreversible fibrosis.* Experientia, 1970. **26**(3): p. 244-245.
14. Ramachandran, P. and J.P. Iredale, *Reversibility of liver fibrosis.* Annals of hepatology, 2009. **8**(4): p. 283-291.
15. Pellicoro, A., P. Ramachandran, and J.P. Iredale. *Reversibility of liver fibrosis*. in *Fibrogenesis & tissue repair*. 2012. BioMed Central.
16. Bataller, R. and D.A. Brenner, *Liver fibrosis.* The Journal of clinical investigation, 2005. **115**(2): p. 209-218.
17. Jiao, J., S.L. Friedman, and C. Aloman, *Hepatic fibrosis.* Current opinion in gastroenterology, 2009. **25**(3): p. 223.
18. Berardis, S., et al., *Use of mesenchymal stem cells to treat liver fibrosis: current situation and future prospects.* World journal of gastroenterology: WJG, 2015. **21**(3): p. 742.
19. Soyer, M.T., R. Ceballos, and J.S. Aldrete, *Reversibility of severe hepatic damage caused by jejunoileal bypass after re-establishment of normal intestinal continuity.* Surgery, 1976. **79**(5): p. 601-604.

20. Friedman, S.L., et al., *Hepatic lipocytes: the principal collagen-producing cells of normal rat liver.* Proceedings of the National Academy of Sciences, 1985. **82**(24): p. 8681-8685.
21. Geerts, A. *History, heterogeneity, developmental biology, and functions of quiescent hepatic stellate cells*. in *Seminars in liver disease*. 2001. Copyright© 2001 by Thieme Medical Publishers, Inc., 333 Seventh Avenue, New ….
22. Préaux, A.M., et al., *Matrix metalloproteinase-2 activation in human hepatic fibrosis regulation by cell-matrix interactions.* Hepatology, 1999. **30**(4): p. 944-950.
23. Pinzani, M., F. Marra, and V. Carloni, *Signal transduction in hepatic stellate cells.* Liver, 1998. **18**(1): p. 2-13.
24. Svegliati-Baroni, G., et al., *Insulin and insulin-like growth factor-1 stimulate proliferation and type I collagen accumulation by human hepatic stellate cells: differential effects on signal transduction pathways.* Hepatology, 1999. **29**(6): p. 1743-1751.
25. Everhart, J.E., *Digestive diseases in the United States: Epidemiology and impact*. 1994: DIANE Publishing.
26. Horowitz, J.M., et al., *Evaluation of hepatic fibrosis: a review from the society of abdominal radiology disease focus panel.* Abdominal Radiology, 2017. **42**(8): p. 2037-2053.
27. Kumar, R., et al., *A practical clinical approach to liver fibrosis.* Singapore medical journal, 2018. **59**(12): p. 628.
28. Schuppan, D. and N.H. Afdhal, *Liver cirrhosis.* The Lancet, 2008. **371**(9615): p. 838-851.
29. Castera, L., X. Forns, and A. Alberti, *Non-invasive evaluation of liver fibrosis using transient elastography.* Journal of hepatology, 2008. **48**(5): p. 835-847.
30. Castéra, L., et al., *Prospective comparison of transient elastography, Fibrotest, APRI, and liver biopsy for the assessment of fibrosis in chronic hepatitis C.* Gastroenterology, 2005. **128(**2): p. 343-350.
31. Friedman, S.L., *Mechanisms of hepatic fibrogenesis.* Gastroenterology, 2008. **134**(6): p. 1655-1669.
32. Bedossa, P. and V. Paradis, *Liver extracellular matrix in health and disease.* The Journal of Pathology: A Journal of the Pathological Society of Great Britain and Ireland, 2003. **200**(4): p. 504-515.
33. Decaris, M.L., et al., *Identifying nonalcoholic fatty liver disease patients with active fibrosis by measuring extracellular matrix remodeling rates in tissue and blood.* Hepatology, 2017. **65(**1): p. 78-88.
34. Su, Q., et al., *MicroRNAs in the pathogenesis and treatment of progressive liver injury in NAFLD and liver fibrosis.* Advanced drug delivery reviews, 2018. **129**: p. 54-63.
35. Everhart, J.E., et al., *Prognostic value of Ishak fibrosis stage: findings from the hepatitis C antiviral long-term treatment against cirrhosis trial.* Hepatology, 2010. **51**(2): p. 585-594.
36. Poynard, T., P. Bedossa, and P. Opolon, *Natural history of liver fibrosis progression in patients with chronic hepatitis C.* The Lancet, 1997. **349**(9055): p. 825-832.
37. Sumida, Y., A. Nakajima, and Y. Itoh, *Limitations of liver biopsy and non-invasive diagnostic tests for the diagnosis of nonalcoholic fatty liver disease/nonalcoholic steatohepatitis.* World journal of gastroenterology: WJG, 2014. **20**(2): p. 475.

38. Braticevici, C.F., et al., *Can We Replace Liver Biopsy with Non-Invasive Procedures?* Liver Biopsy, 2011: p. 225-240.
39. Abdi, W., J.C. Millan, and E. Mezey, *Sampling variability on percutaneous liver biopsy.* Archives of Internal Medicine, 1979. **139**(6): p. 667-669.
40. Regev, A., et al., *Sampling error and intraobserver variation in liver biopsy in patients with chronic HCV infection.* The American journal of gastroenterology, 2002. **97**(10): p. 2614-2618.
41. Ratziu, V., et al., *Sampling variability of liver biopsy in nonalcoholic fatty liver disease.* Gastroenterology, 2005. **128**(7): p. 1898-1906.
42. Poynard, T., V. Ratziu, and P. Bedossa, *Appropriateness of liver biopsy.* Canadian Journal of Gastroenterology and Hepatology, 2000. **14**(6): p. 543-548.
43. Van, D.T., et al., *Liver biopsy. Its safety and complications as seen at a liver transplant center.* Transplantation, 1993. **55**(5): p. 1087-1090.
44. Younossi, Z.M., et al., *Ultrasound-guided liver biopsy for parenchymal liver disease (an economic analysis).* Digestive diseases and sciences, 1998. **43**(1): p. 46-50.
45. Bravo, A.A., S.G. Sheth, and S. Chopra, *Liver biopsy.* New England Journal of Medicine, 2001. **344**(7): p. 495-500.
46. Bhunchet, E. and K. Fujieda, *Capillarization and venularization of hepatic sinusoids in porcine serum-induced rat liver fibrosis: a mechanism to maintain liver blood flow.* Hepatology, 1993. **18**(6): p. 1450-1458.
47. Goodman, Z.D. and K.G. Ishak, *Occlusive venous lesions in alcoholic liver disease: a study of 200 cases.* Gastroenterology, 1982. **83**(4): p. 786-796.
48. Chang, K.-W., et al. *3D biomimetic chip integrated with microvascular system for studying the liver specific functions*. in *2012 7th IEEE International Conference on Nano/Micro Engineered and Molecular Systems (NEMS)*. 2012. IEEE.
49. Naito, M., et al., *Differentiation and function of Kupffer cells.* Medical Electron Microscopy, 2004. **37**(1): p. 16-28.
50. Adachi, Y., et al., *Inactivation of Kupffer cells prevents early alcohol-induced liver injury.* Hepatology, 1994. **20**(2): p. 453-460.
51. Fischer, R., et al., *Caspase 9–dependent killing of hepatic stellate cells by activated Kupffer cells.* Gastroenterology, 2002. **123**(3): p. 845-861.
52. Zeisberg, M., et al., *Fibroblasts derive from hepatocytes in liver fibrosis via epithelial to mesenchymal transition.* Journal of Biological Chemistry, 2007. **282**(32): p. 23337-23347.
53. Shinyashiki, N., et al., *Microwave dielectric study on hydration of moist collagen.* Biopolymers: Original Research on Biomolecules, 1990. **29**(8-9): p. 1185-1191.
54. Hinz, B., et al., *The myofibroblast: one function, multiple origins.* The American journal of pathology, 2007. **170**(6): p. 1807-1816.
55. Desmoulière, A., I.A. Darby, and G. Gabbiani, *Normal and pathologic soft tissue remodeling: role of the myofibroblast, with special emphasis on liver and kidney fibrosis.* Laboratory investigation, 2003. **83**(12): p. 1689-1707.
56. Marieb, E.N. and K. Hoehn, *Human anatomy & physiology*. 2007: Pearson education.
57. Frevert, U., et al., *Intravital observation of Plasmodium berghei sporozoite infection of the liver.* PLoS biology, 2005. **3**(6).
58. Wardle, E.N., *Kupffer cells and their function.* Liver, 1987. **7**(2): p. 63-75.

59. Verrecchia, F. and A. Mauviel, *TGF-β and TNF-α: antagonistic cytokines controlling type I collagen gene expression.* Cellular signalling, 2004. **16**(8): p. 873-880.
60. Klune, J.R., et al., *HMGB1: endogenous danger signaling.* Molecular medicine, 2008. **14**(7-8): p. 476-484.
61. Yang, Q., et al., *The role of intracellular high-mobility group box 1 in the early activation of Kupffer cells and the development of Con A-induced acute liver failure.* Immunobiology, 2013. **218**(10): p. 1284-1292.
62. Suzuki, S., et al., *Role of Kupffer cells and the spleen in modulation of endotoxin-induced liver injury after partial hepatectomy.* Hepatology, 1996. **24**(1): p. 219-225.
63. Dutta-Moscato, J., et al., *A multiscale agent-based in silico model of liver fibrosis progression.* Frontiers in bioengineering and biotechnology, 2014. **2**: p. 18.
64. Brodsky, B. and J.A. Ramshaw, *The collagen triple-helix structure.* Matrix Biology, 1997. **15**(8-9): p. 545-554.
65. Mierke, C.T., et al., *Vinculin facilitates cell invasion into three-dimensional collagen matrices.* Journal of Biological Chemistry, 2010. **285**(17): p. 13121-13130.
66. Parry, D.A., *The molecular fibrillar structure of collagen and its relationship to the mechanical properties of connective tissue.* Biophysical chemistry, 1988. **29**(1-2): p. 195-209.
67. Siegel, R.C. and J. Fu, *Collagen cross-linking. Purification and substrate specificity of lysyl oxidase.* Journal of Biological Chemistry, 1976. **251**(18): p. 5779-5785.
68. Walters, B.D. and J.P. Stegemann, *Strategies for directing the structure and function of three-dimensional collagen biomaterials across length scales.* Acta biomaterialia, 2014. **10**(4): p. 1488-1501.
69. Rappaport, A., et al., *Subdivision of hexagonal liver lobules into a structural and functional unit. Role in hepatic physiology and pathology.* The anatomical record, 1954. **119**(1): p. 11-33.
70. Medzhitov, R., et al., *Highlights of 10 years of immunology in Nature Reviews Immunology.* Nature Reviews Immunology, 2011. **11**(10): p. 693-702.
71. Shapiro, C.N. and H.S. Margolis, *Worldwide epidemiology of hepatitis A virus infection.* Journal of hepatology, 1993. **18**: p. S11-S14.
72. Lai, C.L., et al., *Viral hepatitis B.* The Lancet, 2003. **362**(9401): p. 2089-2094.
73. Poynard, T., et al., *Viral hepatitis C.* The Lancet, 2003. **362**(9401): p. 2095-2100.
74. Swain, S.L., K.K. McKinstry, and T.M. Strutt, *Expanding roles for CD4+ T cells in immunity to viruses.* Nature Reviews Immunology, 2012. **12**(2): p. 136-148.
75. Curtsinger, J.M. and M.F. Mescher, *Inflammatory cytokines as a third signal for T cell activation.* Current opinion in immunology, 2010. **22**(3): p. 333-340.
76. Bao, S., J. Zheng, and G. Shi, *The role of T helper 17 cells in the pathogenesis of hepatitis B virus-related liver cirrhosis.* Molecular medicine reports, 2017. **16**(4): p. 3713-3719.
77. Wang, L., S. Chen, and K. Xu, *IL-17 expression is correlated with hepatitis B-related liver diseases and fibrosis.* International journal of molecular medicine, 2011. **27**(3): p. 385-392.
78. Brand, S., et al., *IL-22 is increased in active Crohn's disease and promotes proinflammatory gene expression and intestinal epithelial cell migration.* American Journal of Physiology-Gastrointestinal and Liver Physiology, 2006. **290**(4): p. G827-G838.

79. McGee, H.M., et al., *IL-22 promotes fibroblast-mediated wound repair in the skin.* Journal of Investigative Dermatology, 2013. **133**(5): p. 1321-1329.
80. Levy, G.A., et al., *The effect of mouse hepatitis virus infection on the microcirculation of the liver.* Hepatology, 1983. **3**(6): p. 964-973.
81. Mueller, S., H.K. Seitz, and V. Rausch, *Non-invasive diagnosis of alcoholic liver disease.* World journal of gastroenterology: WJG, 2014. **20**(40): p. 14626.
82. Mandrup-Poulsen, T., et al., *Cytokines cause functional and structural damage to isolated islets of Langerhans.* Allergy, 1985. **40**(6): p. 424-429.
83. Cave, M., et al., *Nonalcoholic fatty liver disease: predisposing factors and the role of nutrition.* The Journal of nutritional biochemistry, 2007. **18**(3): p. 184-195.
84. Yin, H., L. Sun, and J. Chen, *Micromechanics-based hyperelastic constitutive modeling of magnetostrictive particle-filled elastomers.* Mechanics of materials, 2002. **34**(8): p. 505-516.
85. Vodovotz, Y., et al., *Translational systems biology of inflammation.* PLoS computational biology, 2008. **4**(4).
86. An, G., et al., *Agent-based models in translational systems biology.* Wiley Interdisciplinary Reviews: Systems Biology and Medicine, 2009. **1**(2): p. 159-171.
87. An, G., *In silico experiments of existing and hypothetical cytokine-directed clinical trials using agent-based modeling.* Critical care medicine, 2004. **32**(10): p. 2050-2060.
88. Segovia-Juarez, J.L., S. Ganguli, and D. Kirschner, *Identifying control mechanisms of granuloma formation during M. tuberculosis infection using an agent-based model.* Journal of theoretical biology, 2004. **231**(3): p. 357-376.
89. Tamayo, R.P., *Is cirrhosis of the liver experimentally produced by CC14 an adequate model of human cirrhosis?* Hepatology, 1983. **3**(1): p. 112-120.
90. Bhattacharya, S., et al., *Modeling drug-and chemical-induced hepatotoxicity with systems biology approaches.* Frontiers in physiology, 2012. **3**: p. 462.
91. Wambaugh, J. and I. Shah, *Simulating microdosimetry in a virtual hepatic lobule.* PLoS computational biology, 2010. **6**(4).
92. Dorn, C., J. Heilmann, and C. Hellerbrand, *Protective effect of xanthohumol on toxin-induced liver inflammation and fibrosis.* International journal of clinical and experimental pathology, 2012. **5**(1): p. 29.
93. Clermont, Y., M. Lalli, and Z. Bencsath-Makkai, *Light-microscopic histology atlas.* Saatavilla www-muodossa: http://audilab. bmed. mcgill. ca/HA/html/HAintro_E. html, 2014.
94. Suk, K.T. and D.J. Kim, *Staging of liver fibrosis or cirrhosis: The role of hepatic venous pressure gradient measurement.* World journal of hepatology, 2015. **7**(3): p. 607.
95. Fallatah, H.I., *Noninvasive biomarkers of liver fibrosis: an overview.* Advances in Hepatology, 2014. **2014**.
96. Nassef, Y.E., et al., *Performance of diagnostic biomarkers in predicting liver fibrosis among hepatitis C virus-infected Egyptian children.* Memórias do Instituto Oswaldo Cruz, 2013. **108**(7): p. 887-893.
97. Deffieux, T., et al., *Shear wave spectroscopy for in vivo quantification of human soft tissues visco-elasticity.* IEEE transactions on medical imaging, 2008. **28**(3): p. 313-322.
98. Logan, D.L., *A first course in the finite element method*. 2011: Cengage Learning.

99. Saleh, H.A. and A.H. Abu-Rashed, *Liver biopsy remains the gold standard for evaluation of chronic hepatitis and fibrosis.* Journal of gastrointestinal and liver diseases, 2007. **16**(4): p. 425.
100. Scheuer, P.J., *Liver biopsy size matters in chronic hepatitis: bigger is better.* Hepatology, 2003. **38**(6): p. 1356-1358.
101. Rozario, R. and B. Ramakrishna, *Histopathological study of chronic hepatitis B and C: a comparison of two scoring systems.* Journal of hepatology, 2003. **38**(2): p. 223-229.
102. Bedossa, P. and F. Carrat, *Liver biopsy: the best, not the gold standard.* Journal of hepatology, 2009. **50**(1): p. 1-3.
103. Grimaud, J.-A., et al., *Collagen immunotyping in human liver: light and electron microscope study.* Journal of Histochemistry & Cytochemistry, 1980. **28**(11): p. 1145-1156.
104. Yu, Y., et al., *Deep learning enables automated scoring of liver fibrosis stages.* Scientific reports, 2018. **8**(1): p. 1-10.
105. Vigneri, P., et al., *Diabetes and cancer.* Endocrine-related cancer, 2009. **16**(4): p. 1103-1123.
106. Kalaitzakis, E., et al., *Gastrointestinal symptoms in patients with liver cirrhosis: associations with nutritional status and health-related quality of life.* Scandinavian journal of gastroenterology, 2006. **41**(12): p. 1464-1472.
107. Sandrin, L., et al., *Transient elastography: a new noninvasive method for assessment of hepatic fibrosis.* Ultrasound in medicine & biology, 2003. **29**(12): p. 1705-1713.
108. Garra, B.S., *Clinical elasticity estimation and imaging: applications and standards*, in *Tissue Elasticity Imaging*. 2020, Elsevier. p. 1-19.
109. Zoli, M., et al., *Portal venous flow in response to acute β-blocker and vasodilatatory treatment in patients with liver cirrhosis.* Hepatology, 1986. **6**(6): p. 1248-1251.
110. Ludwig, D., et al., *The postprandial portal flow is related to the severity of portal hypertension and liver cirrhosis.* Journal of hepatology, 1998. **28**(4): p. 631-638.
111. Ludwig, D., et al., *48-Hour hemodynamic effects of octreotide on postprandial splanchnic hyperemia in patients with liver cirrhosis and portal hypertension.* Digestive diseases and sciences, 2000. **45**(5): p. 1019-1027.
112. Nery, F., et al., *Nonselective beta-blockers and the risk of portal vein thrombosis in patients with cirrhosis: results of a prospective longitudinal study.* Alimentary pharmacology & therapeutics, 2019. **49**(5): p. 582-588.
113. Stingl, J., et al., *Morphology and some biomechanical properties of human liver and spleen.* Surgical and radiologic anatomy, 2002. **24**(5): p. 285-289.
114. Bolondi, L., et al., *Liver cirrhosis: changes of Doppler waveform of hepatic veins.* Radiology, 1991. **178**(2): p. 513-516.
115. McAvoy, N., et al., *Differential visceral blood flow in the hyperdynamic circulation of patients with liver cirrhosis.* Alimentary pharmacology & therapeutics, 2016. **43**(9): p. 947-954.
116. Khan, N., et al., *Sonographic Comparison of Mean Velocity of Portal Vein in Liver Cirrhosis and Normal Individuals.* Journal of Health and Medical Sciences, 2018. **1**(1): p. 101-107.
117. Friedman, A. and W. Hao, *Mathematical modeling of liver fibrosis.* Mathematical Biosciences & Engineering, 2017. **14**(1): p. 143-164.